STRUCTURAL AND DYNAMICS STUDIES
OF SURFACTANTS AND MICELLES

By

SAMI KARABORNI

A DISSERTATION PRESENTED TO THE GRADUATE SCHOOL
OF THE UNIVERSITY OF FLORIDA
IN PARTIAL FULFILLMENT OF THE REQUIREMENTS FOR THE
DEGREE OF DOCTOR OF PHILOSOPHY

UNIVERSITY OF FLORIDA

1990

To

my Father

ACKNOWLEDGMENTS

TABLE OF CONTENTS

List of Tables

STRUCTURAL AND DYNAMICS STUDIES OF SURFACTANTS AND
MICELLES

By

Sami Karaborni

May, 1990

Micelles are an important class of molecular aggregates that have growing uses in
industry. Yet there is still an absence of good structural or thermodynamic models due
to the lack of a thorough understanding of micellar behavior and micelle formation.

Micelle structure has long been known to be very complex due to the amphiphilic
nature of surfactants. The presence of ions, hydrocarbon chains and water makes
the micellar aggregate difficult to study theoretically since the contributions from
each factor are not known. Presently there are no single experimental or theoretical
methods that can comprehensively study micelles.

In this work several molecular dynamics simulations have been used to study
both the statics and dynamics of micelles and hydrocarbon droplets as well as the
conformation of alkanes and surfactants in water and nonpolar environments.

Micelle and oil droplet simulations have been performed using a segment force model for intra and intersurfactant interactions while micelle–solvent interactions have been modeled using several field potentials that realistically describe surfactant interactions with polar solvents. Dilute solutions of surfactants and n–alkanes in a monatomic nonpolar fluid and in water were performed using conventional intermolecular interactions.

In general, the results show the insensitivity of micellar structure and chain conformation to micelle–solvent interaction models regardless of chain length or head group characteristics, while aggregate shape was found on the average to be somewhat nonspherical with significant fluctuations.

In all instances the micelle core was found to be like the oil droplet and the chain conformation to be similar to that of surfactants in nonpolar media. In general, local structure results were similar to experimental and other simulation data.

The conformation of alkanes in a fluid of nonpolar segments closely resembles the conformation of surfactants. In addition, alkanes exhibit some characteristics that are independent of chain length, such as the average trans fraction, and other properties that are proportional to chain length, such as radius of gyration and end–to–end distance.

The conformation of ionic surfactants in water was found to be significantly different from that in nonpolar fluids. For example, the trans fraction of ionic surfactants was smaller in water than in the nonpolar segment fluid and in micelles.

CHAPTER 1
INTRODUCTION

Surfactants are an important species of amphiphilic molecules that over the years have received great attention from many industries and researchers. When present at high enough concentrations in certain solvents, some surfactants form complex structures known as micelles. Micelles are an important class of aggregates with wide theoretical and practical use, yet the behavior of micelles in polar fluids is still not well understood. In this study molecular dynamics methods have been used to investigate micellar structure and behavior.

The molecular dynamics method has been shown to be a very useful tool in the study of complex molecular systems and is presently the only method to study both the statics and dynamics of micellar solutions. Nonetheless, no explanation of molecular dynamics methods is given in this thesis, but exact details are found elsewhere (Allen and Tildesley, 1987; Haile, 1980).

The purpose of the present work has been to determine the conformation of model surfactant molecules in nonpolar and polar fluids as well as in micellar solutions, and to study the effect of head group size, surfactant chain length and micelle–solvent interaction models on micellar structure and shape via molecular dynamics.

In chapter 2 a molecular dynamics investigation of the conformation of n-alkanes in a monatomic fluid of methylene segments is described. In particular, properties

1

such as trans fraction, radius of gyration and end–to–end distance have been calculated for seven different chain lengths.

In chapter 3 the conformation of two octyl surfactants and a poly (oxyethylene) head group in a monatomic fluid of methylenes are examined. The conformation of an "ionic methyl" octyl surfactant in water is also considered and the effect of the surfactant molecule on water structure is discussed in Appendix A.

In chapter 4 a complete description of all intramolecular and intermolecular interactions present in micelles and hydrocarbon droplets are given with a summary of all micelle–solvent interaction models used.

In chapter 5 the effects of micelle–solvent interaction models on the internal structure and shape of the model micelles, as well as the conformation of surfactants inside the micelles, are analyzed.

In chapter 6 the effect of surfactant chain length and head group characteristics on the micellar behavior are given, and results are compared with those of a hydrocarbon droplet as well as with experimental and other simulation results.

Finally, In chapter 7 some general conclusions are given along with a few recommendations on future work.

CHAPTER 2
DILUTE N–ALKANE SIMULATIONS

2.1 Background

Over the past few years there have been several molecular simulations and statistical mechanics calculations of model n–alkanes. Molecular dynamics (MD) (Ryckaert and Bellemans, 1975, 1978; Weber, 1978; Edberg et al., 1986, 1987; Wielopolski and Smith, 1986; Toxvaerd, 1987, 1988; Clarke and Brown, 1986; Szczepanski and Maitland, 1983; Rebertus et al., 1979), Monte Carlo (MC) (Jorgensen, 1981a, 1981b; Jorgensen et al., 1981e; Bigot and Jorgensen, 1981; Bãnon et al., 1985), Brownian dynamics (BD) (Van Gunsteren et al., 1981), and statistical mechanics (SM) (Enciso et al., 1989; Zichi and Rossky, 1986a) have been used to determine the conformation of liquid, isolated and dilute n–alkanes. However, none have examined the conformation of long chain molecules mixed with segment molecules, as might be related to dilute polymer/monomer solutions, supercritical extraction and to micelle forming surfactant monomers. Also, little analysis of chain length effect on the conformation of n–alkanes has been made.

Molecular simulation is a powerful tool to investigate the chain conformation, yet results are usually subject to the effect of force field models, computational methods and simulation duration. Previously, molecular simulations have concentrated on short n–alkanes, especially n–butane.

3

Simulations of butane appear to be very simple, since they involve only one di-hedral angle, but they are extremely difficult to run because they require a large amount of computation time for any statistically meaningful conformational results. Despite the abundance of n-butane simulations, there is no clear conclusion about its conformation in liquid or in dilute solutions.

In general, all chain simulations should be carefully undertaken if an analysis on conformation is intended. In particular, special care should be given to the applica-tion of constraints (Toxvaerd, 1987; Rallison, 1979; Helfland, 1979) and preferential sampling methods (Bigot and Jorgensen, 1981).

We report here the results of a series of molecular dynamics of seven different model n–alkanes having from 7 to 21 carbons in Lennard–Jones monatomic fluids, without the application of chain constraints or preferential sampling. The objectives were to study chain length effects on structure and to determine the dominant ef-fects on chain conformation. Results from these simulations may give some insight on the conformations of chains with fewer carbons without actually performing the simulations.

2.2 Chain Model

The interaction potential model used here has been previously applied to micellar aggregates of model chain surfactants (Haile and O'Connell, 1984; Woods et al., 1986). Except for the rotational potential, it is similar to the one described by Weber (1978). The chain molecule is represented by a skeletal chain composed of n equal-diameter

soft spheres representing methyl tails or methylene segments. The bond vibration and angle bending potentials are

$$U_v(b_i) = \frac{1}{2}\gamma_v(b_i - b_0)^2 \tag{2.1}$$

$$U_b(\theta_i) = \frac{1}{2}\gamma_b(\cos\theta_0 - \cos\theta_i)^2 \tag{2.2}$$

where b_i is the bond length between segments i and i+1, b_0 is the equilibrium length, γ_v is the bond vibration force constant, θ_0 is the equilibrium bond angle, θ_i is the angle between segments i, i+1 and i+2, and γ_b is the bending vibration force constant. The bond rotational potential chosen for these simulations is that of Ryckaert and Bellemans (1975):

$$\begin{aligned}U(\phi) &= \gamma_r(\ 1.116 - 1.462\cos\phi - 1.578\cos^2\phi + 0.368\cos^3\phi \\ &\quad +3.156\cos^4\phi + 3.788\cos^5\phi)\end{aligned} \tag{2.3}$$

Following Weber (1978) the intramolecular potential also includes a (6–9) Lennard–Jones interaction between segments on the chain that are separated by at least three carbons, and for all intermolecular interactions.

$$U(r_{ij}) = \epsilon\left[2\left(\frac{r_m}{r_{ij}}\right)^9 - 3\left(\frac{r_m}{r_{ij}}\right)^6\right] \tag{2.4}$$

The parameters are listed in Table 2.1.

Table 2.1: Intermolecular and Intramolecular Potential Parameters.

r_m	ϵ	b_0	θ_0	γ_v	γ_b	γ_r
Å	J/mol	Å	degree	J/(mol Å^2)	J/mol	J/mol
4.00	419	1.539	112.15	9.25×10^5	1.3×10^5	8313

2.3 Simulation Details

In all simulations, a box was created with N_s particles having the size and mass of a methylene group along with the n–alkane in the middle, and periodic boundary conditions were applied to solvent segments. The box boundaries moved with the chain to keep its center of mass always in the middle.

Newton's second differential equations of motion were solved for each of the N_s plus n soft spheres by using a fifth–order predictor–corrector algorithm due to Gear (1971). The number of solvent groups was chosen so that the chain was entirely in the box when fully extended. The time step used in solving the equations of motion was 1.395×10^{-15} secs.

The preparation procedure for all runs was to assign initial positions to all segments including those of the chain, which was not in the all trans conformation. The simulation was then run until equilibrium was reached, and the analysis performed on samples of 105 to 698 picoseconds.

The state conditions for all runs are listed in table 2.2. The temperature is the same for all runs at 298 K, and the reduced density is 0.7 which corresponds to a number density of 0.0109 Å^{-3}.

Table 2.2: Summary of Simulations.

Chain Length	7	9	11	13	15	17	21
Equilibrium Run psec	698	530	209	140	112	140	105
Number of solvent segments	101	99	245	243	485	483	479

2.4 Results

2.4.1 Chain Conformation. Average Trans Bond Fraction.

The trans bond fraction was calculated for the seven different chain lengths and is shown in Table 2.3. In general the trans fraction does not show any trends, and the mean values differ. The uncertainty in all simulations is less than 10%. Although the trans fraction is not constant, the variation among chains is smaller than the statistical fluctuations. An average value of about 69% can be used for all chains from n–butane to n–uneicosane.

The results from our simulations can be compared to those from MD simulations of hydrocarbon fluids, dilute solutions and single molecules, and with BD simulations of single chains as well as statistical mechanics calculations. Comparisons include n–butane (Tables 2.4 and 2.5), n-hexane (Table 2.6), n-octane (Table 2.7) and n–decane (Table 2.8).

The following discussion assumes that the fraction of trans bonds is equal to the average value of 69% for all hydrocarbon chains up to 21 carbons. This value for n–butane is higher than other MD simulations (Ryckaert and Bellemans, 1978; Edberg et al., 1986; Wielopolski and Smith, 1986; Toxvaerd, 1988; Rebertus et al., 1979) and statistical mechanics calculations (Enciso et al., 1989; Zichi and Rossky, 1986a), but comparable to BD (Van Gunsteren et al., 1981) and MC results (Jorgensen 1981a, 1981b; Jorgensen et al., 1981e; Bigot and Jorgensen, 1981; Bãnon et al., 1985). Several factors may have affected the MD work, especially the limited duration of some

Table 2.3: Average Structural Values for All Hydrocarbon Chains

Chain Length	7	9	11	13	15	17	21
% Trans	71	67	68	68	71	68	70
	± 6	± 8	± 9	± 8	± 4	± 7	± 7
$< R >$ Å	6.78	8.19	9.54	11.5	12.4	14.7	16.4
$< R^2 >$ Å^2	52.8	68.4	93.9	135.8	157.4	220.6	286.1
$< S >$ Å	2.18	2.66	3.13	3.63	4.06	4.63	5.36
$< S^2 >$ Å^2	5.82	8.54	11.7	15.9	19.5	26.0	34.7

Table 2.4: Average Values for Neat N–Butane as extrapolated from simulations, and as calculated by Ryckaert and Bellemans (1978), Edberg et al. (1986), Toxvaerd (1988), Jorgensen (1981a), Banon et al. (1985) and Wielopolski and Smith (1986).

Author	Method	Temperature (K)	% Trans
Ryckaert	MD	291	54
Edberg	MD	291	60.6
Toxvaerd	MD	291	62.6
Jorgensen	MC	273	67.1
Bãnon	MC	298	67.5
Wielopolski	MD	285	58.5
Extrapolated	MD	298	69

Table 2.5: Average Values for Single and Dilute N–Butane as extrapolated from simulations, and as calculated by Rebertus et al. (1979), Bigot and Jorgensen (1981), Zichi and Rossky (1986a), Enciso et al. (1989) and Van Gunsteren et al. (1981).

	Rebertus	Bigot	Zichi	Enciso	Van Gunsteren	Extrapolated
Method	MD	MC	SM	SM	BD	MD
T (K)	298	298	298	300	291.5	298
% Trans	57	65	38	58.5	66	69

Table 2.6: Average Values for N–Hexane as extrapolated from Our Linear Fits and as Determined from Other Workers: Clarke and Brown (1986)

	Clarke	Extrapolated
Method	MD	MD
T (K)	300	298
$< R^2 >^{1/2}$ Å	5.56	6.16
% Trans	68	69

Table 2.7: Average Values for N–Octane as Interpolated from Linear Fits and as Determined from Other Workers: Szczepanski and Maitland (1983).

	Szczepanski	Interpolated
Method	MD	MD
T (K)	396	298
$< R >$ Å	7.24	7.59
$< R^2 >^{1/2}$ Å	7.28	7.57
$< S >$ Å	2.59	2.67
$< S^2 >^{1/2}$ Å	2.60	2.67
% Trans	64	69

Table 2.8: Average Values for N–Decane as Interpolated from Linear Fits and as determined by Ryckaert and Bellemans (1978), Edberg et al. (1987), Toxvaerd (1987) and Van Gunsteren et al. (1981).

	Ryckaert	Edberg	Toxvaerd	Van Gunsteren	Interpolated
Method	MD	MD	MD	BD	MD
T (K)	481	481	481	481	298
$< R >$ Å	8.81	–	–	8.64	9.00
$< R^2 >^{1/2}$ Å	8.87	8.87	8.82	8.72	9.06
$< S >$ Å	3.11	–	–	3.07	2.90
$< S^2 >^{1/2}$ Å	3.16	3.11	3.12	3.08	3.18
% Trans	60.4	62.4	62.4	60	69

simulations and the use of constraints on the angles that reduces the rate of trans–gauche transitions (Toxvaerd, 1987). It is also possible that some of the differences between simulations arises from variations in the intermolecular potential models (Bānon et al., 1985).

For pure n–hexane the MD results of Clarke and Brown (1986) at 300 K gave a similar value to ours.

For pure n–octane the only available results are those of Szczepanski and Maitland (1983) at 394 K. They found 64% trans, a value consistent with ours at 298 K.

For n–decane there are several available MD and BD results, but most were performed at high temperatures. Again, however, the somewhat reduced trans fractions are consistent with our lower temperature result.

2.4.2 End–to–End Distance and Radius of Gyration

The end to end distance $< R >$ and the radius of gyration $< S >$ were calculated for the different chains. Figure 2.1 shows how the average end–to–end distance is a linear function of chain length. The standard deviation increases with the carbon number. Figure 2.2 shows that the average radius of gyration for all seven chains is also proportional to the chain length. In tables 2.4–2.8 the radius of gyration and the end–to–end distance from the linear fits are compared to other simulation data. In general the agreement is good, particularly considering the differences in temperature for n–octane and n–decane.
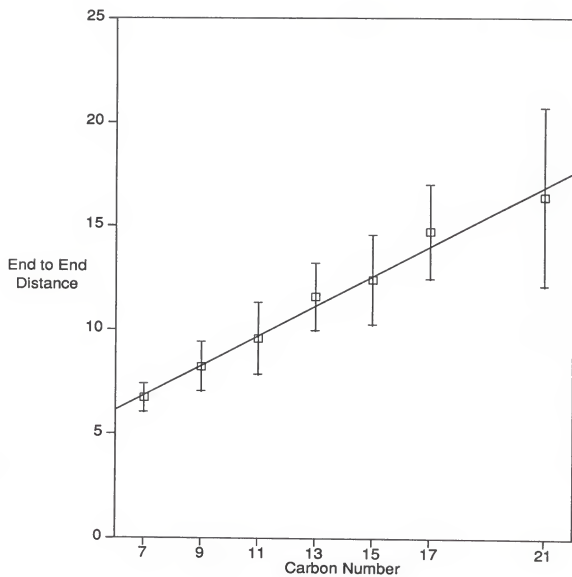
Figure 2.1: The end–to–end distance for hydrocarbon chains as a function of chain length
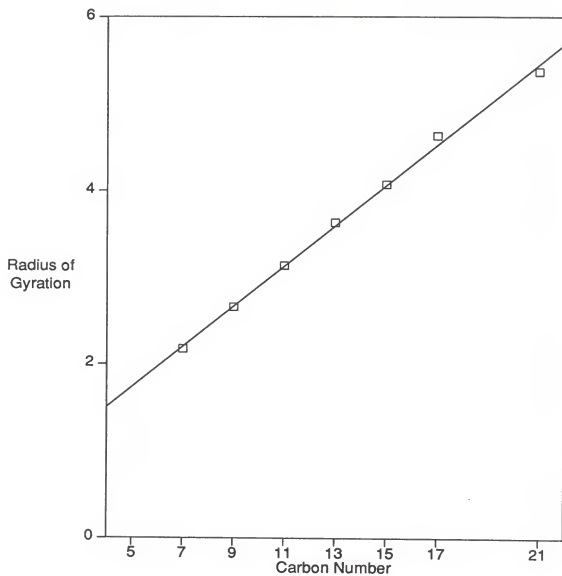
Figure 2.2: The radius of gyration for hydrocarbon chains as a function of chain length

2.4.3 Trans Bond Distribution

Trans bond distributions have been calculated but are of limited quantitative value. Simulations must be significantly longer for any statistically meaningful conclusions to be made. For example, symmetry in the bonds was sometimes not fully reached. However, the analyses can provide some insights.

Several trends can be seen in the distributions of tables 2.9 and 2.11. Table 2.9 shows that for most chain lengths, the most probable number of trans bonds agrees with the average trans fraction. The distribution widens as the chain length decreases, and a few states are rarely reached, especially those with more gauche than trans bonds. The results from these probability distributions can be used to calculate a conformational entropy associated with the runs as measured by

$$S/k = -\sum_{i=0}^{n-3} p_i \ln p_i \tag{2.5}$$

where p_i is the probability of finding a number of bonds, i, in the trans conformation, and $n - 3$ is the number of dihedral angles on a chain of n segments. The uniform distribution entropy resulting in the highest conformational entropy can also be calculated:

$$S/k = \ln(n - 2) \tag{2.6}$$

The ratio of equations 2.5 and 2.6 is a measure of randomness with respect to the uniform distribution with a value of unity showing maximum randomness. Values for

Table 2.9: Probability of Finding a Given Number of Trans Bonds on the Chain.

Number of Trans Bonds	7	9	11	13	15	17	21
0	0.00	0.00	0.00	0.00	0.00	0.00	0.00
1	0.01	0.01	0.00	0.00	0.00	0.00	0.00
2	0.30	0.09	0.00	0.00	0.00	0.00	0.00
3	0.51	0.20	0.03	0.00	0.00	0.00	0.00
4	0.18	0.34	0.22	0.02	0.00	0.00	0.00
5		0.32	0.28	0.11	0.00	0.05	0.00
6		0.05	0.22	0.23	0.01	0.00	0.00
7			0.24	0.37	0.11	0.04	0.00
8			0.01	0.22	0.38	0.26	0.01
9				0.05	0.38	0.22	0.03
10				0.00	0.11	0.30	0.07
11					0.02	0.09	0.16
12					0.00	0.04	0.24
13						0.00	0.17
14						0.00	0.16
15							0.08
16							0.05
17							0.02
18							0.00
$-\sum p_i \ln p_i$	1.06	1.44	1.50	1.51	1.35	1.67	2.00

the entropy ratio for all chain lengths is shown in Table 2.10. The entropy ratio of the chains in dense LJ fluid is not affected by chain length (about 0.65 ± 0.06), even though longer chains have larger numbers of available states and might be expected to have a much higher entropy ratio. Apparently, all chains have the same constraint from reaching some of the states such as the $g^{\pm}g^{\mp}$ conformations. These were shown by Pitzer (1940) to be unfavored by an overlapping called the "pentane interference."

Table 2.11 shows that within the statistics of ± 0.03 the probability of finding a dihedral angle in trans conformation is essentially equal for all angles on the chain. The uncertainties can be estimated from comparing results for bonds in the same position relative to the chain end. In particular there seem to be no trends of probabilities from the ends to the middle of the chains.

The probability distributions can be used to calculate another conformational entropy for the different alkane chains, using p_i in equation 2.5 as the probability of a particular dihedral angle, i, to be in trans conformation. Figure 2.3 shows that the entropy is equal to the logarithm of the number of states, $n - 3$, confirming the equiprobability of all angles to be in trans conformation.

2.5 Conclusions

The conformation of isolated chains of segments in fluids of segments at liquid densities have been examined by molecular dynamics. The trans fraction is about 2/3 with uniform distribution among the dihedral angles.

Table 2.10: Randomness of Conformation: Ratio of Equations 2.5 and 2.6.

Chain Length	7	9	11	13	15	17	21
$-\sum p_i \ln p_i$	1.06	1.44	1.50	1.51	1.35	1.67	2.00
$\ln(n-2)$	1.61	1.95	2.20	2.40	2.56	2.71	2.94
$\frac{-\sum p_i \ln p_i}{\ln(n-2)}$	0.66	0.74	0.68	0.63	0.53	0.62	0.68

Table 2.11: Probability of Finding a Particular Dihedral Angle in the Trans Conformation.

Dihedral Angle	7	9	11	13	15	17	21
ϕ_1	0.25	0.15	0.11	0.11	0.06	0.03	0.05
ϕ_2	0.26	0.19	0.16	0.12	0.12	0.07	0.05
ϕ_3	0.25	0.15	0.12	0.11	0.07	0.08	0.07
ϕ_4	0.24	0.18	0.13	0.08	0.11	0.06	0.03
ϕ_5		0.15	0.13	0.13	0.09	0.07	0.05
ϕ_6		0.18	0.06	0.08	0.07	0.08	0.07
ϕ_7			0.16	0.11	0.05	0.08	0.07
ϕ_8			0.13	0.09	0.08	0.05	0.08
ϕ_9				0.05	0.07	0.07	0.04
ϕ_{10}				0.13	0.09	0.08	0.08
ϕ_{11}					0.08	0.10	0.03
ϕ_{12}					0.11	0.08	0.05
ϕ_{13}						0.05	0.08
ϕ_{14}						0.10	0.05
ϕ_{15}							0.03
ϕ_{16}							0.07
ϕ_{17}							0.05
ϕ_{18}							0.06
Uniform	0.25	0.17	0.13	0.10	0.08	0.07	0.06
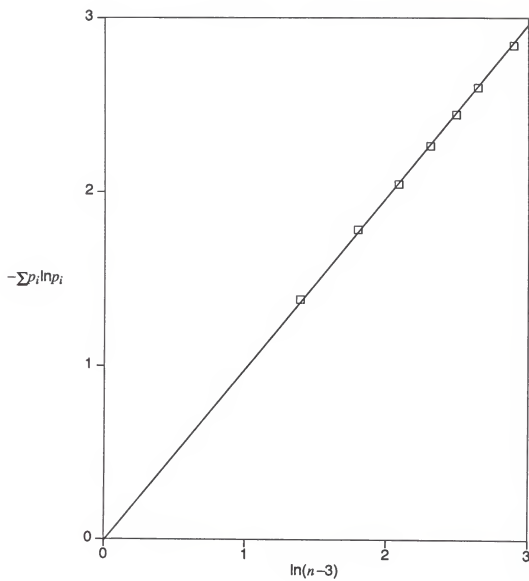
Figure 2.3: Entropy $S/k = -\sum p_i \ln p_i$ is plotted as a function of $\ln(n-3)$. For an n-alkane there are n-3 dihedral bonds and p_i is the probability of finding a bond in trans conformation.

The end–to–end distance and radius of gyration are linear functions of chain length for chains of 7 to 21 segments.

CHAPTER 3
SIMULATIONS OF SURFACTANTS IN A LENNARD–JONES FLUID
OF SEGMENTS AND IN WATER

3.1 Background

In the last chapter we have discussed the conformation of n–alkanes, and have shown some important properties of n–alkanes. In this chapter we direct our attention to the study of ionic and nonionic surfactants. Surfactants are an important class of molecules due to their amphiphilic behavior. They are used in the formation of many colloidal solutions, and have applications in enhanced oil recovery, detergency, catalysis and many other industries, however there has been no detailed simulation studies of dilute surfactant solutions. A conformational study of free surfactants is particularly important for comparison with micellar surfactants, as well as with free alkanes and those in hydrocarbon droplets.

Many experimental studies of micellar solutions and thermodynamic studies of micelles have claimed that surfactant chains change conformation upon micellization by making the trans fraction higher in micelles than in hydrocarbon fluids or water. To date, no well documented molecular simulations have been performed to verify this assertion.

In this chapter a series of molecular dynamics simulations have been performed to study the conformation of an octyl "ionic methyl" surfactant in a Lennard–Jones

fluid of methylene segments and in water, and an octyl "nonionic sulfate" surfactant in a Lennard–Jones fluid of segments. We also describe a simulation of a nonionic surfactant head group (poly (oxyethylene)) in a Lennard–Jones fluid of segments.

3.2 Potential Model for Segmented Molecules

3.2.1 Octyl Surfactants

The interaction potential model for the surfactant used in these simulations, except for rotational effects, is similar to the one described by Weber (1978). The surfactant molecule is represented by a skeletal chain composed of 8 equal-diameter soft spheres each representing a methyl tail or methylene segment and a soft sphere representing the head group (Figure 3.1). The bond vibration and angle bending potentials for groups other than the head group are those of Weber (1978) taken from a simulation of n–butane.

$$U_v \left(b_i \right) = \frac{1}{2} \gamma_v \left(b_i - b_0 \right)^2 \tag{3.1}$$

$$U_b \left(\theta_i \right) = \frac{1}{2} \gamma_b \left(\cos \theta_0 - \cos \theta_i \right)^2 \tag{3.2}$$

where b_i is the bond length between segments i and i+1, b_0 is the equilibrium length, γ_v is the bond vibration force constant, θ_0 is the equilibrium bond angle, θ_i is the angle between segments i, i+1 and i+2, and γ_b is the bending vibration force constant. The bond rotational potential chosen for these simulations is that of Ryckaert and Bellemans (1975):
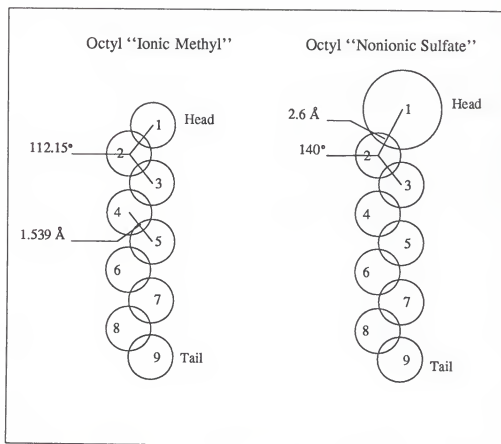
Figure 3.1: Model octyl surfactants.

$$U\left(\phi\right) = \gamma_r(\quad 1.116 - 1.462 \cos \phi - 1.578 \cos^2 \phi + 0.368 \cos^3 \phi$$

$$+3.156 \cos^4 \phi + 3.788 \cos^5 \phi) \tag{3.3}$$

The intramolecular potential also includes a (6–9) Lennard–Jones interaction between segments on the chain that are separated by at least three carbons.

For $j - i > 3$:

$$U_{LJ}\left(r_{ij}\right) = \epsilon \left[2 \left(\frac{r_m}{r_{ij}}\right)^9 - 3 \left(\frac{r_m}{r_{ij}}\right)^6 \right] \tag{3.4}$$

The parameters involving all segments on the octyl "ionic methyl" and the octyl "nonionic sulfate" surfactants (Muller et al., 1968) are listed in Table 3.1.

3.2.2 Poly (Oxyethylene) Molecule

The model used for the poly (oxyethylene) chain is composed of six oxyethylene segments. As shown in Figure 3.2 each oxyethylene segment is a –CH2–CH2–O. The first carbon on the poly (oxyethylene) has three hydrogens and the last oxygen on the chain has one hydrogen. Nineteen soft spheres with different sizes and masses were made to represent methyl, methylene and oxygen groups. The hydrogen atom attached to the last oxygen on the chain is also represented by a soft sphere. All groups interact via bond vibration, angle bending and rotation, as well as (6–12) Lennard–Jones and electrostatic interactions between groups that are separated by at least three groups.

Table 3.1: Bond Parameters of "Methylene" and "Sulfate" Groups. "Sulfate" Parameters are Used when an Intramolecular Interaction Involves a "Nonionic Sulfate" Head Group. "Methylene" Parameters are Used with All Other Intramolecular Interactions.

Parameter	"Methylene" Value	"Sulfate" Value	Units
b_0	1.539	2.6	Å
θ_0	112.15	140	degree
γ_v	9.25×10^5	2.7×10^4	J/(mol Å²)
γ_b	1.3×10^5	9.1×10^5	J/mol
γ_r	8313	20000	J/mol
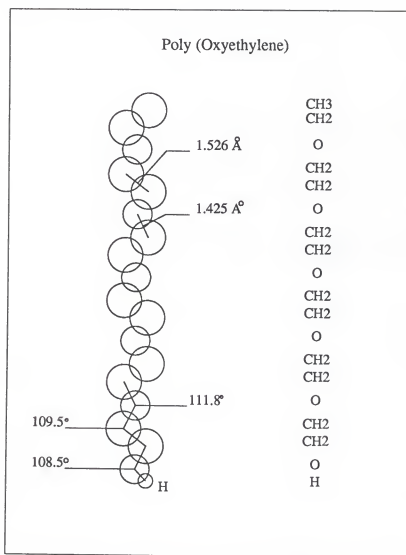
Figure 3.2: Model poly (oxyethylene) molecule.

For $j - i > 3$:

$$U\left(r_{ij}\right) = \frac{q_i q_j e^2}{r_{ij}^2} + 4\epsilon \left[\left(\frac{\sigma}{r_{ij}}\right)^{12} - \left(\frac{\sigma}{r_{ij}}\right)^6 \right] \tag{3.5}$$

The values for coulombic interaction parameters (Table 3.2) are similar to those by Jorgensen (1981c) from a study of alcohols and ethers.

The bond vibration and angle bending parameters were those extracted from molecular mechanical studies by Weiner et al. (1987) and used in equations 3.1 and 3.2. The rotational potential is from a Monte Carlo study of n–alkyl ethers by Jorgensen and Ibrahim (1981d):

$$V(\phi) = D_0 + D_1 \cos\phi + D_2 \cos 2\phi + D_3 \cos 3\phi \tag{3.6}$$

A complete list of intramolecular parameters is given in Tables 3.3, 3.4 and 3.5.

3.3 Interaction Models for Molecules in a Lennard–Jones Fluid of Segments and Simulation Details

In simulations involving the "ionic methyl" and "nonionic sulfate" surfactants in a Lennard–Jones fluid of segments a Lennard–Jones (6–9) potential (equation 3.4) is used for all surfactant segment–fluid segment interactions. In addition a coulombic interaction is used to model the head group–counterion attraction in the case of the "ionic methyl" simulation.

$$U\left(r_{ij}\right) = \frac{q_i q_j e^2}{r_{ij}^2} \tag{3.7}$$

As shown in Table 3.6 all segments on the surfactant or in the fluid have the same Lennard–Jones parameters except the "nonionic sulfate" surfactant head group which has different parameters.

Table 3.2: Lennard–Jones and Coulombic Interaction Parameters for Poly (oxyethylene).

Site	q electrons	ϵ J/mol	σ Å
CH2,CH3	0.29	480	4
O	-0.58	811	3.05
O (of OH)	-0.69	811	3.05
H	0.40	0	0

Table 3.3: Bond Parameters for Poly (oxyethylene).

Bond	γ_v J/(mol Å^2)	b_0 Å
CH2–CH2	9.25×10^5	1.526
CH2–O	1.14×10^6	1.425
O–H	1.97×10^6	0.960

Table 3.4: Angle Parameters for Poly (oxyethylene).

Angle	γ_b J/mol	θ_0 degree
CH2–CH2–O	1.651×10^5	109.5
CH2–O–CH2	2.067×10^5	111.8
CH2–O–H	1.135×10^5	108.5

Table 3.5: Torsion Parameters for Poly (oxyethylene).

Bond	γ_r J/mol	D_0	D_1	D_2	D_3
CH2–CH2–O–CH2	8314	1.053	1.250	0.368	0.675
O–CH2–CH2–O	8314	1.078	0.355	0.068	0.791
CH2–CH2–O–H	8314	1.053	1.250	0.368	0.675

Table 3.6: Intermolecular Potential Parameters for "Methylene" and "Sulfate" Groups. "Sulfate" Parameters are Used when an Intermolecular Interaction Involves a "Nonionic sulfate" Head Group. "Methylene" Parameters are Used with All Other Intermolecular Interactions.

Parameter	"Methylene" Value	"Sulfate" Value	Units
r_m	4.0	10	Å
ϵ	419	419	J/mol
q_i	-1	0	electrons

In the poly (oxyethylene) simulation a Lennard–Jones (6–12) potential plus an electrostatic interaction is used to model all pair potentials.

In each of the simulations involving an octyl surfactant a box with 108 particles each with a size and mass of a methylene group was created, then 9 particles in the middle of the box are replaced by the surfactant chain. In the octyl "ionic methyl" surfactant simulation, one methylene group is also replaced by a counterion that has the same intermolecular potential as other solvent groups, but with a positive charge of 1e. When the simulation is started the surfactant chain is not in the all–trans conformation, and periodic boundary conditions are applied to the solvent segments and to the counterion, but not to the surfactant molecule. The box is moved according to the movements of the surfactant molecule so that its center of mass is always in the middle.

In the simulation involving the poly (oxyethylene) chain, the simulation box included 500 particles of which 19 were replaced by the poly (oxyethylene) molecule.

Newton's second differential equations of motion were solved for all segments in the solvent and on the chain by using a fifth–order predictor–corrector algorithm due to Gear (1971).

All simulation runs consisted of a large number of steps until equilibrium was reached as determined by constant average energy and temperature. A sample of subsequent time steps is then used to calculate the average properties. Simulation details for all runs are shown in Table 3.7

Table 3.7: Simulation Details for Runs in Lennard–Jones Fluid of Segments.

Simulation	Time Step secs	Equilibration Steps	Equilibrium Run
"ionic methyl" surfactant	1.395×10^{-15}	50,000	150,000
"nonionic sulfate" surfactant	1.395×10^{-15}	40,000	130,000
poly (oxyethylene)	1.331×10^{-15}	10,000	75,000

3.4 Results for Molecules in a Lennard–Jones Fluid of Segments

In this section we report results on end–to–end distance and radius of gyration distributions, and the probability distribution of the number of bonds in trans fraction, and the probability of a bond to be in trans fraction. Average values for the trans fraction, end–to–end distance and radius of gyration are also reported.

3.4.1 Average and Mean Values

In Tables 3.8, 3.9 and 3.10 we show the average and mean values for trans fractions, end-to-end distances and radii of gyration. The trans percentage for both the "ionic methyl" and "nonionic sulfate" surfactants is about $73\pm6\%$. A value that is similar to the trans fraction of nonane in dilute solution (see chapter 2) and that in micelles of "polar methyl" and "nonionic sulfate" surfactants (see chapters 5 and 6). The trans fraction in poly (oxyethylene) is $46\pm1\%$ indicating a mostly gauche conformation. Apparently neither the size of the head group on the octyl "nonionic sulfate" surfactant nor the added negative charge on the head group of the octyl "ionic methyl" surfactant have an effect on the average trans fraction as compared to a 9–carbon n–alkane. On the other hand the trans fraction for poly (oxyethylene) is considerably different from the corresponding 19–carbon n–alkane. There may be several factors affecting the conformation of this molecule, but the dominant one is probably the presence of charges on different segments of the molecule. The distribution of charges on the chain yield several extra interactions such as dipole–dipole, quadrupole–quadrupole, hydrogen bonding or any combination of these interactions.

Table 3.8: Average Properties for the Octyl "Ionic Methyl" Surfactant in a Lennard–Jones Fluid of Segments.

Property	Value	Units
% Trans	74 ± 6	
$< R >$	8.20	Å
$< R^2 >$	68.7	Å^2
$< S >$	2.70	Å
$< S^2 >$	8.76	Å^2

Table 3.9: Average Properties for the Octyl "Nonionic Sulfate" Surfactant in a Lennard–Jones Fluid of Segments.

Property	Value	Units
% Trans	73 ± 5	
$< R >$	9.96	Å
$< R^2 >$	100.	Å^2
$< S >$	3.53	Å
$< S^2 >$	16.1	Å^2

Table 3.10: Average Properties for Poly (Oxyethylene) in a Lennard–Jones Fluid of Segments.

Property	Value	Units
% Trans	46 ± 1	
$< R >$	11.9	Å
$< R^2 >$	148.	Å^2
$< S >$	4.13	Å
$< S^2 >$	20.2	Å^2

The larger Lennard–Jones energy parameters for chain oxygen and different rotational potentials for oxygens and methylenes also would lead to differences between the 19–carbon n–alkane conformation and that of poly (oxyethylene).

The end–to–end distance and radius of gyration for the octyl "ionic methyl" surfactant are similar to those of the 9–carbon n–alkane (see chapter 2), while the "nonionic sulfate" surfactant shows a larger end–to–end distance and radius of gyration. Apparently the presence of a negative charge on the "ionic methyl" surfactant head group has little effect on these quantities in contrast to the influence of head group size and mass. The radius of gyration shows a 26% increase for the "nonionic sulfate" surfactant over that of the "ionic methyl" surfactant. Part of this disparity in radius of gyration could be accounted for by the mass of the head group which is seven times that of the "ionic methyl" surfactant head group, and by the longer chain from end to end when in the all–trans conformation. Additionally the mean end–to–end distance for the "nonionic sulfate" molecule is 21% larger than that of the "ionic methyl" surfactant mainly because small separations are not accessible (see below). The end–to–end distance and the radius of gyration for the poly (oxyethylene) molecule are much smaller than for the corresponding 19–carbon n–alkane, suggesting a bunched up conformation consistent with a small average trans fraction.

3.4.2 End–to–end Distance

The plot for the end–to–end distance of the "ionic methyl" surfactant is shown in Figure 3.3. The distribution is skewed, though it has a single most probable peak.
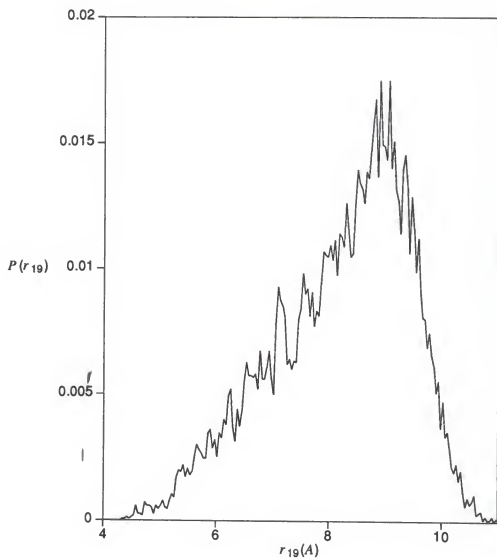
Figure 3.3: End–to–end distribution for the octyl "ionic methyl" surfactant in a Lennard–Jones fluid of segments.

Several small peaks arising from allowed and forbidden conformations are present. The most probable value for the end–to–end distance is higher than the average value.

The end–to–end distance distribution for the "nonionic sulfate" surfactant is shown in figure 3.4. This distribution is also skewed. The occurrence of small peaks is not as frequent as in the distribution for the "ionic methyl" surfactant. In both cases, extra peaks in the distributions at distances below the peak are sharper than those above the peak.

The end–to–end distance distribution for the "ionic methyl" surfactant chain extends from quite small distances of 4Å to 11Å. Basically the end–to–end distance samples all available conformational space from 4Å (r_{min} in the Lennard–Jones potential) to 11Å (the all–trans end–to–end distance).

The end–to–end distance distribution for the "nonionic sulfate" surfactant extends from about 7Å to about 12.3Å. Here again the long range part of the distribution is indicative of the all–trans end–to–end distance, while the short range part is indicative of the head and tail approaching each other to r_{min} in the Lennard–Jones potential.

Figure 3.5 shows that the end–to–end distance for the poly (oxyethylene) molecule is a fairly symmetric distribution which reaches from values around the Lennard–Jones σ to values less than the all–trans end–to–end distance. The difference between the average and the most probable values of the end–to–end distance is less than 5 %. The short range limit indicates that hydrogen bonding may occur between the terminal
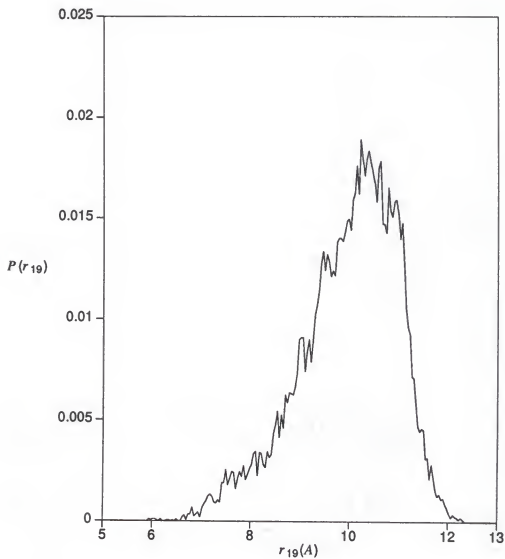
Figure 3.4: End–to–end distribution for the octyl "nonionic sulfate" surfactant in a Lennard–Jones fluid of segments.
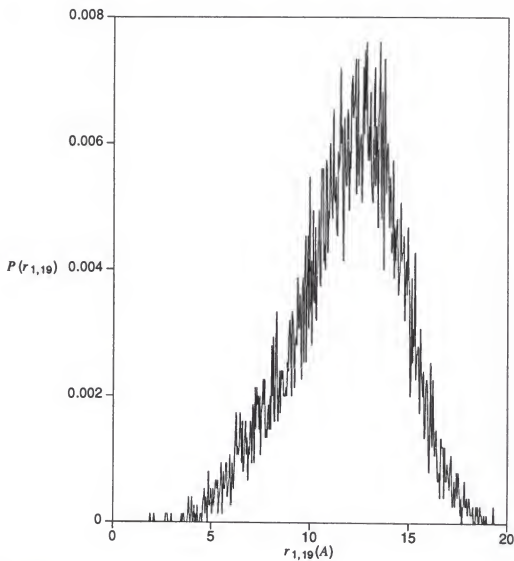
Figure 3.5: End–to–end distribution for poly (oxyethylene) in a Lennard–Jones fluid of segments.

hydrogen atom and the first occurring oxygen atom on the other side of the molecule. Several sharp peaks are present, a result of the observed motions of the chain among its 16 bonds (which should be compared to only 6 for the octyl surfactants). The distribution has large amplitude spikes, particularly around the peak.

3.4.3 Radius of Gyration

In figures 3.6, 3.7 and 3.8 are shown the radii of gyration for all three simulations. The radius of gyration distributions for the "ionic methyl" and the "nonionic sulfate" surfactants are fairly symmetric and smooth with some small peaks at discrete positions on the chains, indicating different conformations. The difference in both simulations between the average and most probable values of the radius of gyration is less than 2%. The radius of gyration distribution for the poly (oxyethylene) molecule is not symmetric, and has a distinctive shoulder at 3.6 Å, while the main peak occurs at 4.2 Å. There are also many more extra peaks than for the octyl surfactants. The particular conformation of the shoulder in this distribution is uncertain; it could be due to dipole–dipole, quadrupole–quadrupole, charge–charge or hydrogen bonding interactions.

3.4.4 Probability of Finding a Number of Bonds in the Trans Conformation.

The probabilities of finding a number of bonds in the trans conformation for simulations in the Lennard–Jones fluid of segments are shown in Tables 3.11, 3.12 and 3.13.

(In the analysis that follows, a bond is considered to be in trans conformation if $\cos(\phi_i)$ in equations 3.3 and 3.6 is less than -0.5. For all other values of $\cos(\phi_i)$ the
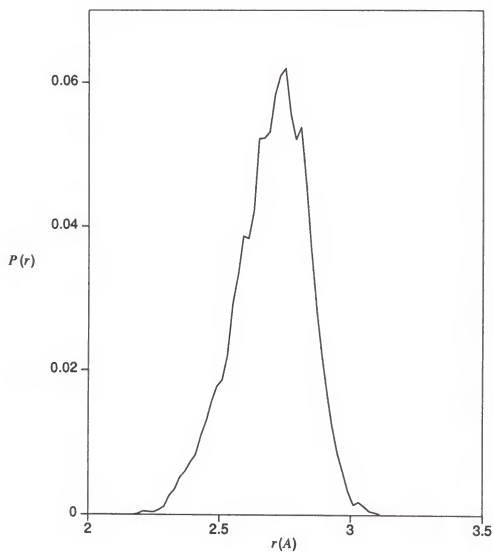
Figure 3.6: Radius of gyration distribution for the octyl "ionic methyl" surfactant in Lennard-Jones fluid of segments.
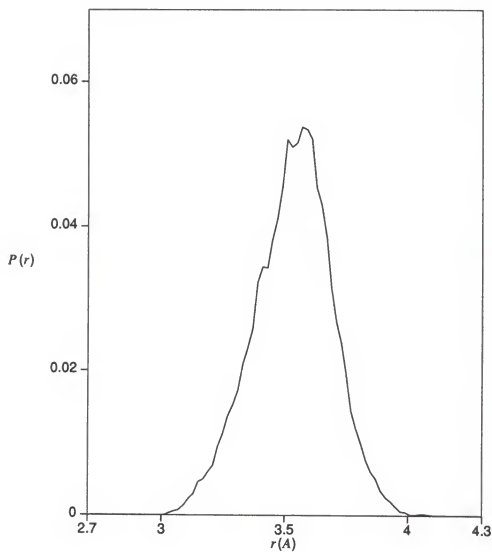
Figure 3.7: Radius of gyration distribution for the octyl "nonionic sulfate" surfactant in a Lennard–Jones fluid of segments.
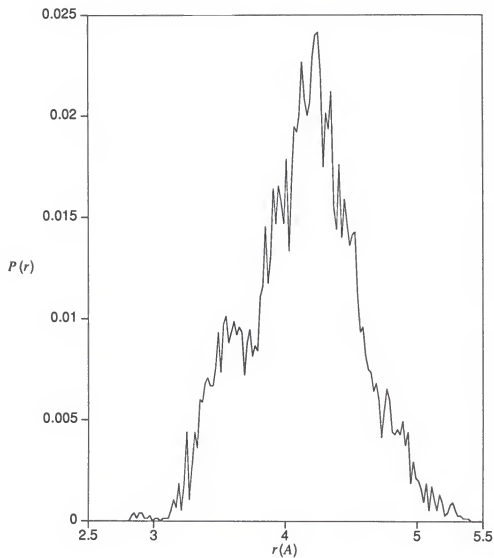
Figure 3.8: Radius of gyration distribution for poly (oxyethylene) in a Lennard–Jones fluid of segments.

Table 3.11: Probability of Finding a Number of Bonds in the Trans Conformation on the Octyl "Ionic Methyl" Surfactant.

Number of bonds	0	1	2	3	4	5	6
Probability	0.0	0.0	0.0	0.12	0.39	0.44	0.05

Table 3.12: Probability of Finding a Number of Bonds in the Trans Conformation on the Octyl "Nonionic Sulfate" Surfactant.

Number of bonds	0	1	2	3	4	5	6
Probability	0.00	0.00	0.03	0.12	0.33	0.51	0.01

bond is considered gauche.) This probability is similar for both octyl surfactants indicating that states with high gauche conformations are not accessible, while states with one or two gauche bonds are the most probable.

The trans bond probability distribution for poly (oxyethylene) is fairly symmetric, and states with 7 or 8 trans bonds are most probable. This probability is consistent with the average trans fraction found earlier.

3.4.5 Probability of Finding a Particular Bond in the Trans Conformation.

This particular probability looks at each bond separately. The results for this particular property have significant statistical uncertainty due to large fluctuations in the average values. The standard deviation on these values can be as high as the average values. Nonetheless it can be seen that all bonds on the "ionic methyl" surfactant have a similar probability to be in the trans conformation (Table 3.14). The probability of being in trans conformation for each single bond on the "nonionic sulfate" surfactant is highest for bond 1 (bond involving head groups and segments 2, 3 and 4) and then follows a somewhat decreasing probability toward the tail (Table 3.15). This result is probably due to different head group mass, size and rotational potential.

Table 3.16 shows that torsional bonds on poly (oxyethylene) of the groups X–C–O–X (1,2,4,5,7,8,10,11,13,14,16) generally have a higher probability to be in the trans conformation than bonds of the goups X–C–C–X (3,6,9,12,15). The exception is at

Table 3.13: Probability of Finding a Number of Bonds in the Trans Conformation on a Poly (Oxyethylene).

Number of Bonds	0	1	2	3	4	5	6	7	8
Probability	0.0	0.0	0.0	0.01	0.04	0.09	0.15	0.21	0.21
Number of Bonds	9	10	11	12	13	14	15	16	
Probability	0.16	0.08	0.03	0.01	0.0	0.0	0.0	0.0	

Table 3.14: Probability of Finding a Particular Bond in the Trans Conformation on the Octyl "Ionic Methyl" Surfactant.

Bond Number	1	2	3	4	5	6
Probability	0.14	0.19	0.18	0.15	0.17	0.18

Table 3.15: Probability of Finding a Particular Bond in the Trans Conformation on the Octyl "Nonionic Sulfate" Surfactant.

Bond Number	1	2	3	4	5	6
Probability	0.23	0.19	0.18	0.15	0.12	0.13

Table 3.16: Probability of Finding a Particular Bond in the Trans Conformation on the Poly (Oxyethylene) Molecule in a Lennard–Jones Fluid of Segments.

Bond Number	1	2	3	4	5	6	7	8
Probability	0.07	0.07	0.05	0.07	0.07	0.06	0.07	0.07
Bond Number	9	10	11	12	13	14	15	16
Probability	0.06	0.07	0.07	0.06	0.06	0.08	0.04	0.05

the terminal hydrogen end (bond 16) where the hydrogen bonding probably affects the conformation.

3.5 Octyl "Ionic Methyl" Surfactant in Water

3.5.1 Model

In the previous sections of this chapter and in chapter 2 we have discussed the simulation of solutes in a Lennard–Jones fluid of segments. In this section we turn our attention to simulations of aqueous solutions. Simulations involving water are usually uncertain since there is no generally valid potential for water. Rather, there are several effective pair potentials such as the BF (Bernal and Fowler, 1933), ST2 (Stillinger and Rahman, 1974, 1978), MCY (Matsuoka et al., 1976), SPC (Berendsen et al., 1981), TIPS (Jorgensen, 1981c), TIPS2 (Jorgensen, 1982), and TIP4P (Jorgensen et al., 1983). Overall the SPC, ST2, TIPS2 and TIP4P models give reasonable structural and thermodynamic descriptions of liquid water (Jorgensen et al., 1983), but the simplicity of SPC from a computational point of view makes it attractive. It is not clear yet which model predicts the best dynamics, though it seems that SPC has a slight edge over TIPS2 and TIP4P (Strauch and Cummings, 1989; Alper and Levy, 1989) in predicting the dielectric constant. Consequently the SPC potential is used here to model water.

The octyl "ionic methyl" surfactant molecule is similar to the one described in 3.2.1 except that the interactions between chain segments are modeled by a (6–12) Lennard–Jones potential instead of the (6–9) potential. This should not affect the

conformation of the surfactant since the excluded volume effects for n–butane have been modeled equally well by an r^{-12} or an r^{-9} contribution to the Lennard–Jones potential (Weber, 1978; Ryckaert and Bellemans, 1978), and no difference was found here for surfactants in micelles (see below). The water potential used was originally given by Berendsen et al. (1981), and consists of two parts: 1) a soft sphere interaction between oxygen atoms on the water molecule and 2) a coulombic potential that involves oxygen–oxygen, oxygen–hydrogen and hydrogen–hydrogen interactions.

$$U\left(r_{ij}\right) = \frac{q_i q_j e^2}{r_{ij}} + 4\epsilon \left[\left(\frac{\sigma}{r_{ij}}\right)^{12} - \left(\frac{\sigma}{r_{ij}}\right)^{6}\right] \tag{3.8}$$

Effectively the SPC model consists of 10 interactions, of which one is Lennard–Jonesian while the remaining nine contributions are coulombic.

In our present model for the dilute solution of the octyl "ionic methyl" surfactant, there are basically six kinds of interactions: 1) the water–water interaction which is modeled by the SPC potential; 2) the water–chain segment interaction which is modeled by a (6–12) Lennard–Jones term; 3) the water–head group interaction that is modeled by a Lennard–Jones interaction plus a coulombic term to account for charges on the surfactant head and the water molecules; 4) the water–counterion interaction that is modeled similar to the water–head group interaction; 5) the head group–counterion interaction that is similar to the water–counterion interaction; 6) the chain segment–counterion interaction which is modeled by a (6–12) Lennard–Jones potential.

The parameters for all the potentials are shown in Table 3.17. These parameters were used earlier by Jönsson et al. (1986) in their study of an octyl surfactant micelle. The counterion has the size of a sodium ion, while the head group is a methyl–sized segment that is negatively charged.

The simulation techniques chosen here are different from those described in prior simulations. In particular the bonds and angles in the water molecule are held rigid using a quaternion method (Evans, 1977). A fourth order predictor–corrector method is used to solve the translational and rotational equations of motion, and a gaussian thermostat is used to keep a constant temperature.

In this simulation the box contained 206 water molecules, one counterion and the octyl "ionic methyl" chain. The surfactant molecule is free to wonder around the box. Periodic boundary conditions are applied to all molecules including the surfactant. There is no clear way on how to apply periodic boundary conditions to the surfactant molecule once one of its segments leaves the main box. Therefore, when this occurred the simulation was stopped and restarted from the previous configuration with the surfactant molecule moved to the middle of the box. The minimum image criteria is used to evaluate all interactions, except for interactions on the surfactant chain, and a spherical cutoff distance is used for all short and long range interactions. This apparently crude assumption was used in the original development of the SPC model.

The time step used in this simulation (0.5 fs) is relatively short compared to prior simulations. The run proceeded with 20000 time steps until the usual criteria of

56 56

Table 3.17: Lennard-Jones Parameters for Interacting Atoms and Segments. σ is Given in Å and ϵ is Given in J/mol. Net Charges are Given in Units of the Elementary Charge $e=1.602\times10^{-19}$esu.

σ	chain segment	head group	oxygen on water	sodium ion	hydrogen on water
Chain segment	3.92	3.92	3.279	2.667	0.00
head group		3.92	3.279	2.667	0.00
oxygen on water			3.165	2.667	0.00
sodium ion				2.667	0.00
hydrogen on water					0.00
ϵ	chain segment	head group	oxygen on water	sodium ion	hydrogen on water
Chain segment	697	697	702	313	0.00
head group		697	702	313	0.00
oxygen on water			650	313	0.00
sodium ion				313	0.00
hydrogen on water					0.00
$q_i q_j$	chain segment	head group	oxygen on water	sodium ion	hydrogen on water
Chain segment	0.00	0.00	0.00	0.00	0.00
head group		1.00	0.82	-1.00	-0.41
oxygen on water			0.672	-0.82	-0.336
sodium ion				1.00	0.41
hydrogen on water					0.168

equilibrium was reached followed by an additional 39000 time steps to calculate the equilibrium and dynamic properties of the solution.

3.5.2 Results

The average values for the end–to–end distance, the radius of gyration and the trans fraction are shown in Table 3.18. The trans percentage for the "ionic methyl" surfactant in water is 60%. This value is significantly different from the trans fraction of the octyl "ionic methyl" surfactant in a Lennard–Jones fluid of segments (see section 3.4.1) and the "polar methyl" octyl surfactant in micelles (see chapter 6). Apparently the presence of an aqueous solvent significantly affects the surfactant conformation. The average end–to–end distance and the radius of gyration for the "ionic methyl" surfactant in water are similar to those of the same surfactant in the Lennard–Jones fluid of segments, but the distribution and most probable values are significantly different in the two cases. In general, the average results are consistent with the concept of chain straightening upon micellization.

Plots for the end–to–end distance and the radius of gyration are shown in Figures 3.9 and 3.10. The end–to–end distribution is irregular though fairly symmetric. There are two major peaks near 8.4 Å with several other peaks at shorter distances. When compared to the end–to–end distribution for the octyl "ionic methyl" surfactant in a Lennard–Jones fluid of segments, the distribution is narrower, and does not reach either the all–trans end–to–end distance or the Lennard–Jones parameter σ. The large gauche fraction explains the first effect and a possible explanation for the

Table 3.18: Average Properties for the Octyl "Ionic Methyl" Surfactant in Water.

Property	Value	Units
% Trans	60 ± 3	
$< R >$	8.18	Å
$< R^2 >$	67.4	Å^2
$< S >$	2.59	Å
$< S^2 >$	8.07	Å^2
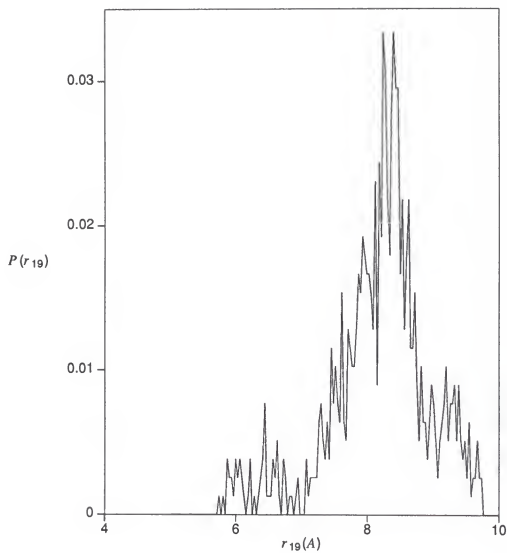
Figure 3.9: End–to–end distribution for the octyl "ionic methyl" surfactant in water.
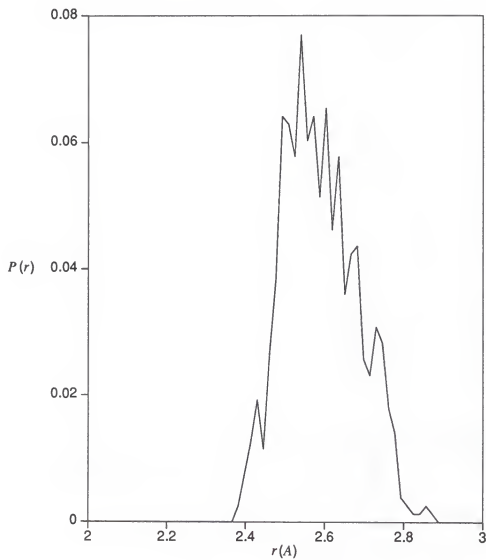
Figure 3.10: Radius of gyration distribution for the octyl "ionic methyl" surfactant in water.

short range difference could be the presence of water molecules that are consistently around the negatively charged head group preventing close contact with the tail segment. Thus, there is a peak at 6.5 Å corresponding to the distance between two methylene segments separated by a water molecule. The presence of other waters around the head may force the distance to be larger than 7Å.

The radius of gyration distribution is fairly symmetric, but has several more peaks and is narrower than the corresponding distribution in the Lennard–Jones fluid of segments. Its slight skewness is towards shorter distances rather than longer ones as in the Lennard–Jones fluid. Such details of the difference between segments and water environments are uncertain.

The probability of a number of bonds to be in the trans conformation and the probability of a bond to be trans are shown in Tables 3.19 and 3.20. From Table 3.19 it can be seen that all states are accessible except the all–gauche conformation, and states with two or three gauche bonds have the highest probabilities. The distribution is similar to that of Table 3.11 for the Lennard–Jones fluid but the number of bonds is decreased by one with the all–trans configuration being quite improbable.

It can be seen in Table 3.20 that all bonds have about the same probability to be in trans conformation. Thus, the water solvent shows no bond preference as does the Lennard–Jones fluid.

Table 3.19: Probability of Finding a Number of Bonds in the Trans Conformation on the Octyl "Ionic Methyl" Surfactant in Water.

Number of Bonds	0	1	2	3	4	5	6
Probability	0.00	0.04	0.09	0.31	0.42	0.14	0.02

Table 3.20: Probability of Finding a Particular Bond in the Trans Conformation on the Octyl "Ionic Methyl" Surfactant in Water.

Bond Number	1	2	3	4	5	6
Probability	0.19	0.15	0.16	0.14	0.20	0.17

3.6 Conclusions

From these simulations of surfactant molecules, it is apparent that ionic surfactants in nonionic fluids behave differently from those in water. In particular the surfactant conformation is more trans in nonpolar fluids (73%) than in water (60%). The conformation of ionic surfactants in a Lennard–Jones fluid of segments is very similar to that of a hydrocarbon chain of corresponding length regardless of head group size, mass and charge. The conformation of surfactants in micelles (chapters 5 and 6) is more like that in nonionic fluids than in water. On the other hand simulations involving poly (oxyethylene) in a Lennard–Jones fluid of segments show that the gauche conformation is preferred (46% trans), and that the distribution of bond orientations is considerably different from that of a model methylene chain.

CHAPTER 4
MODEL MICELLE

4.1 Background

Micelles are an important class of aggregates with wide theoretical and practical
use, yet the behavior of micelles in polar fluids is still not well understood. Over the
past few years, considerable experimental work has examined micellar structure, mi-
celle shape and fluctuations, the micellar chain conformations, and water penetration
in the micelle core.

Experimental methods that are used to study the micellar behavior involve spec-
troscopic techniques such as Small Angle Neutron Scattering (SANS) (Bendedouch
et al., 1983a, 1983b; Tabony, 1984; Cabane et al., 1985; Chen, 1986; Hayter and Pen-
fold, 1981; Hayter and Zemb, 1982; Hayter et al., 1984), Nuclear Magnetic Resonance
(NMR) (Cabane, 1981; Chevalier and Chachaty, 1985; Ulmius and Lindmann, 1981;
Zemb and Chachaty, 1982), Light Scattering (Candau, 1987; Chang and kaler, 1985),
Luminescence Probing (Zana, 1987), Spin Labeling (Taupin and Dvolaitzky, 1987)
and X–ray Scattering (Zemb and Charpin, 1985).

Due to the limitations of some spectroscopic techniques on resolution of time and
space, and the wide distribution of micellar size and shape in solution (Ben–Shaul
and Gelbart, 1985; Degiorgio, 1983), experimental results often disagree. At present

Small–Angle Scattering is the only method that allows distances to be measured in the range 5 to 500 Å (Cabane, 1987). It has been suggested that SANS, particularly with careful isotropic substitution, is the most promising technique for the study of local structure, degree of water penetration in the micelle core, and micellar shape.

Although NMR may be the most powerful and versatile spectroscopic technique for studying systems in the liquid state, the interpretation of primary spectroscopic data is difficult (Lindmann et al., 1987). In fact, NMR is only unambiguous in describing the chain conformation (Cabane et al., 1985).

Micelles have been also studied by structural models. Many of the modeling efforts suggest a structure that differs from the original "pincushion" image of Hartley (1935), but most models make simplifying assumptions ranging from a simple "matchstick" construction (Fromherz, 1981) and a "brush heap" configuration (Menger, 1979, 1985) to a more complex statistical lattice theory (Dill, 1982, 1984a, 1985; Dill and Flory 1980, 1981; Dill et al., 1984b; Cantor and Dill, 1984) and an equal density micelle model (Gruen, 1981, 1985a, 1985b). Unfortunately, the quantitative, and even qualitative model descriptions of micelle behavior may not be accurate because of the assumptions used in their development and the apparent complexity of the micelle structure.

There also have been a few attempts to study micelle structure by computer simulations, mainly Molecular Dynamics and Monte Carlo simulations. The advantage of computer simulations over structural models and experimental methods is that their

only assumption involves the intramolecular and intermolecular potentials while detailed molecular information can be obtained. Haan and Pratt (1981a, 1981b) used Monte Carlo Methods to simulate a micelle with a mean interaction between surfactants. Molecular Dynamics simulations have attempted to model the micelle–solvent interaction without including a solvent (Haile and O'Connell, 1984; Woods et al., 1986; Farrell, 1988) while Jönsson et al. (1986) and Watanabe et al. (1988) have simulated sodium octanoate micelles of 15 members in model water. The results from all simulations appeared to be different, apparently because of their use of different force field models and computational methods.

4.2 Micelle Models

The model used in these simulations is similar to the one described in Woods et al. (1986): a skeletal chain composed of 8 equal–diameter soft spheres for the methyl tail or methylene segments and a soft sphere for the head group. Methyl, methylene segments and head group on the same chain interact via bond vibrational, bending (Weber, 1978) and torsional forces (Ryckaert and Bellemans, 1975) as well as a (6–9) Lennard–Jones potential between segments that are separated by at least three carbons (See Chapter 2).

The intermolecular interactions can be modeled by using five potentials. The different interactions are shown in figure 4.1. Segment–segment and head–segment interactions are modeled by a pairwise additive Lennard–Jones (6–9) form,
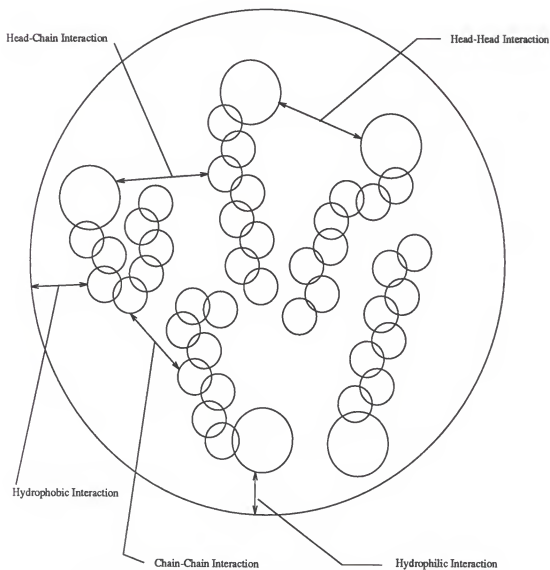
Figure 4.1: Model for intermolecular interactions in micelles

$$U_{LJ}\left(r_{ij}\right) = \epsilon \left[2\left(\frac{r_m}{r_{ij}}\right)^9 - 3\left(\frac{r_m}{r_{ij}}\right)^6\right] \tag{4.1}$$

For head-segment interactions the radius of the minimum potential, r_m, is adjusted to account for the difference between the diameter of the head group and that of the chain segment:

$$r_m^{head-segment} = \frac{1}{2}\left(r_m + r_{hh}\right) \tag{4.2}$$

Head–head interactions are modeled by a purely repulsive potential which includes both dipole–like repulsion and excluded volume effects:

$$U_{hh}\left(r_{ij}\right) = \epsilon \left[2\left(\frac{r_{hh}}{r_{ij}}\right)^3 + 3\left(\frac{r_{hh}}{r_{ij}}\right)^{12}\right] \tag{4.3}$$

The micelle–solvent interactions are not modeled on a particle basis. Rather, the surfactant molecules are surrounded with a varying thickness spherical shell used to mimic a polar solvent. The micelle–solvent interactions can be divided into two contributions, the chain–solvent and head–solvent interactions.

4.2.1 Chain–Solvent Interaction

Two models are proposed to account for the chain–solvent interaction (Figure 4.2). First, an r^{-12} potential on a spherical shell whose center is the aggregate center of mass was applied on the methyl and methylene segments to prevent chains from leaving the micelle

$$U_{cs}^{*(1)}\left(r\right) = \left(r_{cs}^* - r^*\right)^{-12} \tag{4.4}$$
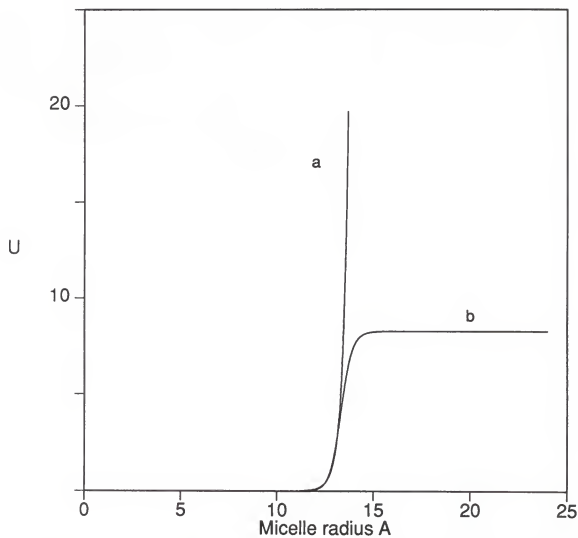
Figure 4.2: Chain–solvent interaction models **a)** $\left(r^*_{wall} - r^*\right)^{-12}$ potential **b)** finite energy barrier, $U^* = U/\epsilon, \epsilon = 419J/mol$

This potential was previously used by Woods et al. (1986) and Farrell (1988). It is considered to be unrealistic because it assumes that methylene segments are completely insoluble in water.

A more realistic approach has been to impose a finite barrier on the hydrocarbon chain that mimics the barrier for solubilization of methylene in water (Vilallonga et al., 1982).

$$U_{cs}^{*(2)}(r) = \kappa / \left(1. + \rho \left(r^*/r_{cs}^*\right)^\tau\right) \tag{4.5}$$

This potential changes rapidly from zero in the core to a higher value outside the core. The value of κ was chosen to match the free energy of solubilization of methylenes in water (Vilallonga et al., 1982), while the steepness of the potential was controlled by ρ and τ to make 90% of the change in 4.5 (Å) as suggested by neutron scattering (Hayter and Penfold, 1981) ($\rho = 0.76$ and $\tau = -46$). This potential is more realistic than the infinite wall potential and allows methylene segments to leave the aggregate.

4.2.2 Head–Solvent Interaction

Three models have been used to account for the head–solvent interactions (Figure 4.3). First, there was the harmonic potential (Woods et al., 1986; Farrell, 1988) about an equilibrium radial position to limit head group movement to a short distance normal to the micelle surface, with free movement along the micelle–solvent boundary.

$$U_{hs}^{*(1)}(r) = \gamma \left(r_{hs}^* - r^*\right)^2 \tag{4.6}$$

The harmonic potential constant γ controls the amplitude of normal movement of
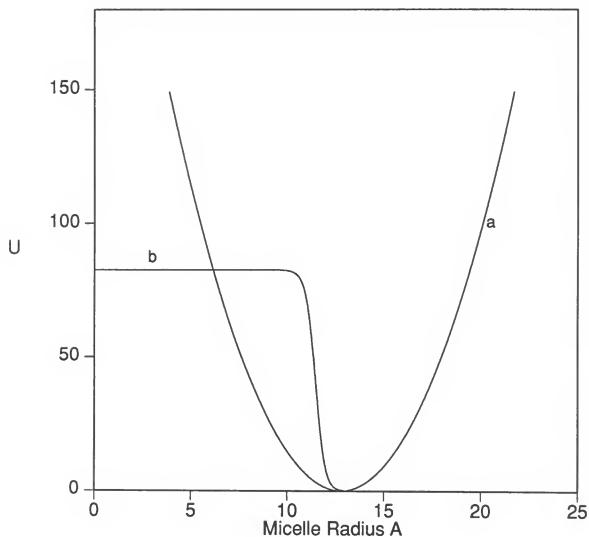
Figure 4.3: Head–solvent interaction models **a)** harmonic potential **b)** finite energy barrier. Half harmonic potential has same form as harmonic potential for a radius less than the equilibrium radius, and is equal to zero for a radius greater than the equilibrium radius. $U^* = U/\epsilon, \epsilon = 419 J/mol$

the head groups, effectively controlling the interfacial area. The application of this potential implies that head groups prefer the interfacial area over both the micelle core and the bulk solvent. Although it can be true that head groups prefer polar over nonpolar environment, it is not known if head groups prefer the interface over the bulk solvent. Assuming that the bulk solvent is as equally favorable to heads as is the interface, two other potentials have been used.

A half–harmonic potential was used to put a high energy barrier on head groups from the micelle side, and no energy barrier imposed from the solvent side.

$$\left.\begin{aligned} u_{hs}^{*(2)}(r) &= \gamma \left(r_{hs}^* - r^* \right)^2 & r^* \leq r_{hs}^* \\ u_{hs}^{*(2)}(r) &= 0. & r^* \geq r_{hs}^* \end{aligned}\right\} \tag{4.7}$$

As with equation 4.6, the value of the repulsive energy at the center of the shell is $\gamma\ r_{hs}^{*2}$. Although this model has the required characteristics, the potential is not twice differentiable at r_{hs}^*.

Finally, a continuously differentiable potential that imposed a finite energy barrier on head groups from the micelle side and no energy barrier from the bulk solvent side was used.

$$u_{hs}^{*(3)}(r) = \beta / \left(1. + \rho \left(2 - r^* / r_{hs}^* \right)^{\tau} \right) \quad r^* < 2 r_{hs}^* \tag{4.8}$$

The values of ρ and τ were chosen to provide a sharp (4.5 Å) transition while β controlled the barrier height. In particular, values of the order of the segment hydrophobic barrier and of the dehydration free energy of head groups (Vilallonga et al., 1982) were used. The potential changes rapidly from zero in the bulk solvent to a

higher value in the micelle core, and is more realistic than the harmonic potential in that the heads do not feel a continuously changing repulsion either inside the micelle or in the solvent.

All parameter values for the micelle-solvent interaction models are in units of r_m, the radius that corresponds to the minimum of the segment–segment (6–9) Lennard–Jones potential, and of ϵ, the energy value for the potential minimum.

4.3 Simulations

Molecular Dynamics simulations of seven model micelles and one hydrocarbon droplet were performed using the above models. In each of the runs, one chain–solvent interaction potential was combined with one head–solvent interaction potential to complete the micelle force field.

Run 1. A micelle of 24 octyl "nonionic sulfate" monomers with the weak harmonic potential of equation 4.6 ($\gamma = 30$) applied to head groups, and the infinite wall potential of equation 4.4 for the chain–shell interactions.

Run 2. A micelle of 24 octyl "nonionic sulfate" monomers with a stronger harmonic potential ($\gamma = 300$) applied to the head groups. The solvophobic potential of equation 4.5 was applied to the segments ($\kappa = 8.27$).

Run 3. A micelle of 24 octyl "nonionic sulfate" monomers with the half–harmonic potential of equation 4.7 ($\gamma = 300$) applied to the head groups. The potential energy for chain segments was the solvophobic potential of run 2.

Run 4. A micelle of 24 octyl "nonionic sulfate" monomers with the potential of

equation 4.8 ($\beta = 8.27$) applied to the head groups. This value of β gives the same barrier for head groups into the core as for segments into the solvent. The head group energy at the center is about $1/360$ that of run 3. The segment potential was the solvophobic potential of run 2.

Run 5. A micelle of 24 octyl "nonionic sulfate" monomers with the potential of equation 4.7 applied to the head groups. The value of β was an order of magnitude greater ($\beta = 82.7$) an estimate of the free energy of transfer of sulfate groups from an aqueous to a hydrocarbon environment. The segment potential was the was the solvophobic potential of run 2.

Run 6. A micelle of 24 octyl "nonionic sulfate" monomers with the head group and segment potentials the same as run 5, but at a high pressure of about 1 bar.

Run 7. A micelle of 24 octyl "polar methyl" monomers with the head group potential of equation 4.6 ($\gamma = 30$), and the chain segment potential was the solvophobic potential of run 2.

Run 8. A hydrocarbon droplet with 24 nonyl chains with the finite barrier segment potential of equation 4.5. The head–head and head–solvent interactions used in the model micelles are segment interactions.

The parameters of equations 4.1–4.8 for all simulations are listed in Table 4.1. These eight simulations provide a basis to check the effect of micelle–solvent models, head group characteristics and chain length on the micellar behavior, and provide a base for comparison between micelles and hydrocarbon droplets.

Table 4.1: Intermolecular Potential Parameters. ϵ_{hh}, γ and β Are in Units of ϵ. r_{hh}, r_{hs}^* and r_{cs}^* are in Units of r_m.

Run	run 1	run 2	run 3	run 4	run 5	run 6	run 7	run 8
$\epsilon(J/mol)$	419	419	419	419	419	419	419	419
r_m (Å)	4.0	4.0	4.0	4.0	4.0	4.0	4.0	4.0
σ (Å)	3.5	3.5	3.5	3.5	3.5	3.5	3.5	3.5
ϵ_{hh}	1	1	1	1	1	1	1	–
r_{hh}	2.45	2.45	2.45	2.45	2.45	2.45	1	–
γ	30	300	300	–	–	–	30	–
κ	–	8.27	8.27	8.27	8.27	8.27	8.27	–
r_{hs}^*	3.2	3.2	3.2	4.72	4.72	2.85	3.00	–
r_{cs}^*	4.2	4.2	3.35	4.2	4.2	3.35	3.50	3.48
β	–	–	–	8.27	82.7	82.7	–	–

System preparation for all runs. Newton's second differential equations of motion were solved for each of the 216 soft spheres by using a fifth–order predictor–corrector algorithm due to Gear (1971). The time step used in solving the equations of motion was equivalent to 1.5 fs for runs 1–6 and 2.0 fs for runs 7–8.

The procedure used in preparing all micelle runs started with initial positions of all segments on each chain in the all–trans conformation and the head group centers distributed about a sphere about twice the final micelle size. The initial steps of the simulation consisted of decreasing the radius of the micelle from the initial to the intended radius while applying an infinite wall potential (Equation 4.4) on the chains and the appropriate head group potential. During the initial steps, the rotational barrier was decreased to one tenth the desired value, and then raised to the final value. The next steps in the micelle simulation changed the chain–solvent interaction to the intended models and fine–tuned the micelle–solvent interaction models radii, r_{cs}^* and r_{hs}^*, to reach the intended pressure (Woods et al., 1986). Finally 12000 time steps constituted the equilibrium run. The same procedure was used in preparing the hydrocarbon droplet simulation.

The state conditions for all runs are listed in table 4.2. The temperature was 298 K in all cases.

Table 4.2: Temperatures and Pressures for Molecular Dynamics Simulations.

Run	1	2	3	4	5	6	7	8
Temp (K)	298	298	298	298	298	298	298	298
Pressure (atm)	≈ 0	≈ 0	≈ 0	≈ 0	≈ 0	≈ 1	≈ 0	≈ 0
No. of Molecules	24	24	24	24	24	24	24	24
Packing Fraction[a]	0.70	0.70	0.70	0.70	0.70	0.70	0.70	0.70

[a]. Packing fraction is $\frac{N\sigma^3\pi}{6V}$

CHAPTER 5
EFFECTS OF MICELLE–SOLVENT INTERACTION

In this chapter we describe the effect of the micelle–solvent interaction models on the micelle behavior by comparing six molecular dynamics simulations of "nonionic sulfate" micelles (Runs 1–6) that have the same inter and intramolecular potentials but different micelle–solvent interaction models.

5.1 Local Structure. Probability Distributions

The primary measures of local structure are the probability distributions of segments. The singlet probability $P_i(r)$ can be determined directly from the simulation by:

$$P_i(r) = \frac{<N_i(r)>}{N} \tag{5.1}$$

Where $<N_i(r)>$ is the average number over time of groups i that are found in shell of thickness δr with radius r, and N is the total number of molecules, with the sum over all shells being:

$$\sum_j <N_i(r_j)> = N \tag{5.2}$$

and

$$\sum_j P_i(r_j) = 1 \tag{5.3}$$

The singlet density $\rho_i(r)$ is related to $P_i(r)$ by:

$$P_i(r) = \frac{\rho_i(r)4\pi r^2 \Delta r}{N} \tag{5.4}$$

When $\Delta r \longrightarrow 0$

$$\int \rho_i(r)4\pi r^2 dr = N \tag{5.5}$$

Thus, a convenient form to use is $r^2 \rho_i(r)$, which is within a multiplicative constant of the true probability $P_i(r)$, and yields an area under the curve that is proportional to N. This particular form is a good basis for comparison between runs.

Results for the tail group distributions for runs 1–6 are shown in figure 5.1. The curves for all six runs are very similar, suggesting that neither the chain–solvent nor the head–solvent models affect the tail distributions. In all cases, tail groups have a finite probability of being found at any distance from the aggregate center, including the micelle surface.

Results for the middle group (segment 5) distributions are shown in figure 5.2. The effect of micelle-solvent interaction models can be seen. Although the peak for all curves occurs at about the same distance from the micelle radius, the heights vary among the runs. In particular, the curves with the harmonic head–solvent models (run 1 and run 2) exhibit a higher peak than the rest of the curves. The height of these curves increases with increasing harmonic constant γ, i.e., the segments peak height increases with greater limitations on the head motion about its equilibrium position. Middle segments, like tail groups, have a finite probability of being found everywhere in the micelle, but the distribution is not as wide as the tail group distribution.
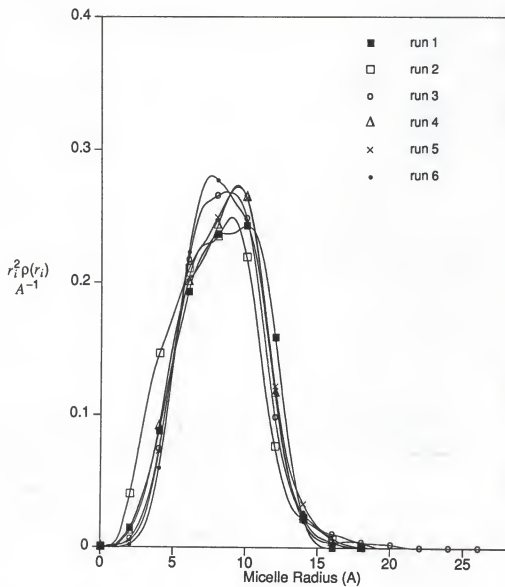
Figure 5.1: Group probability distributions for tail groups
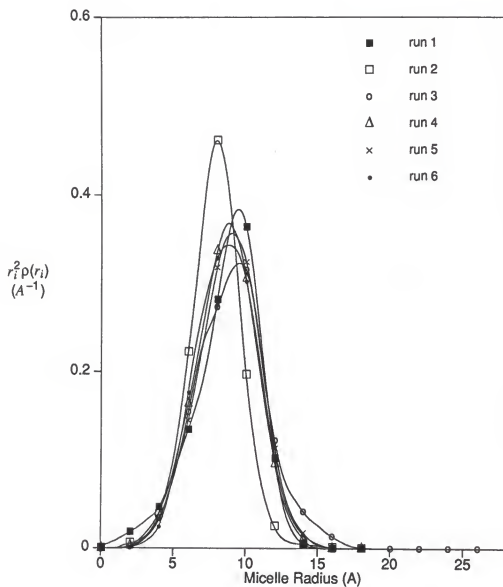
Figure 5.2: Group probability distributions for middle segments (segment 5 from the top of the chain with the head group numbered 1 and the tail group 9)

The effect of micelle–solvent models is greatest for the head group distributions (Figure 5.3). In this plot, neither the positions nor the height of the peaks are similar, and some of the curves exhibit multiple peaks. Again runs 1 and 2 have the highest peaks. In all runs, the head groups are predominately in the palisade region, but some are found in the micelle core. Runs with a finite energy barrier tend to have lower primary peaks, and have second peaks at the micelle center. Even the run with the half harmonic potential shows a small peak at the micelle center. This particular result may be caused by head group repulsion forcing heads to be in the micelle core and the chains need not be fully stretched to fill the core space. This is unlike previous work (Haile and O'Connell, 1984; Woods et al., 1986) where the heads were small, and movement into the center would not yield such energy and entropy advantages for the system.

5.2 Average Positions of Groups

Further information is given on the local structure of groups by calculating the average and the mean radial position for each group. The average radial position, $\bar{R}_i$, and the mean radial position, $(\bar{R}_i^2)^{1/2}$, for each group relative to the aggregate center of mass are calculated by

$$\bar{R}_i = \frac{1}{N} \int \rho_i(r) r_i 4\pi r^2 dr \tag{5.6}$$

$$\bar{R}_i^2 = \frac{1}{N} \int \rho_i(r) r_i^2 4\pi r^2 dr \tag{5.7}$$

The results shown in Tables 5.1 and 5.2 do not show a sizable difference among the runs. On the average, the tail groups are further from the center of mass than
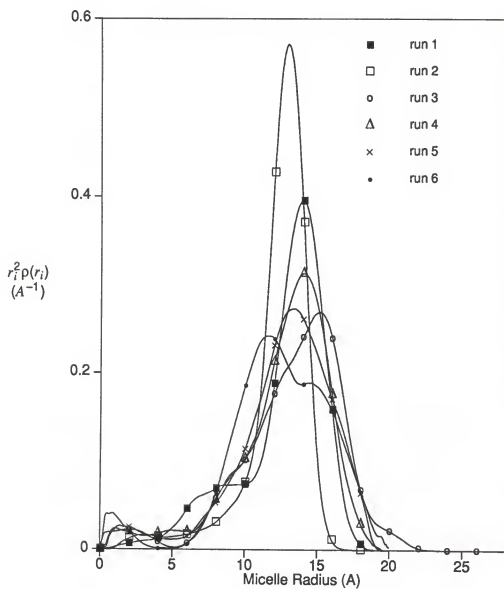
Figure 5.3: Group probability distributions for head groups

Table 5.1: Average Radial Position $\bar{R}_i$ for Each Group, Measured Relative to the Aggregate Center of Mass

group no	run 1	run 2	run 3	run 4	run 5	run 6
1	12.6	12.2	13.2	12.6	12.5	12.4
2	10.6	10.1	11.2	10.6	10.6	10.6
3	9.7	9.2	10.4	9.8	9.7	9.8
4	9.1	8.5	9.7	9.1	9.1	9.2
5	8.6	7.9	9.1	8.6	8.4	8.7
6	8.3	7.6	8.7	8.2	8.2	8.3
7	8.2	7.4	8.4	8.2	7.9	8.3
8	8.2	7.4	8.4	8.2	8.0	8.3
9	8.5	7.7	8.5	8.4	8.4	8.5

Table 5.2: Mean Radial Position $\left(\bar{R}_i^2\right)^{1/2}$ for Each Group, Measured Relative to the Aggregate Center of Mass

group no	run 1	run 2	run 3	run 4	run 5	run 6
1	13.0	12.4	13.7	13.0	12.9	12.9
2	10.9	10.2	11.6	10.9	10.9	10.9
3	10.0	9.3	10.7	10.1	10.0	10.1
4	9.4	8.6	10.0	9.3	9.3	9.4
5	8.9	8.1	9.4	8.8	8.5	8.9
6	8.6	7.8	9.0	8.5	8.3	8.6
7	8.5	7.7	8.7	8.4	8.1	8.5
8	8.6	7.8	8.7	8.5	8.2	8.5
9	8.9	8.1	8.9	8.7	8.8	8.8

are segments 6, 7 and 8. The results from run 2 differ slightly in that all segments are closer to the center. This result is probably due to the strong head group harmonic potential keeping the head on the surface of the micelle, and forcing segments into the core at smaller average radial positions. Also, the half harmonic potential has the opposite effect because head groups can easily move away from the micelle. Therefore the average positions of all groups in run 3 are slightly higher than in the other runs.

5.3 Distributions of tail groups

Another measure of local structure is the distribution of tail groups as determined from scattering amplitudes of tails (a Fourier transform of the singlet density $\rho_i(r)$).

$$\frac{A(Q)}{A(0)} = 4\pi \int r\rho_i(r)\frac{\sin(rQ)}{Q}dr \qquad (5.8)$$

Figure 5.4 presents the scattering amplitude for tails in runs 1–6. The simulation results show very good agreement for all runs except run 2.

5.4 Distribution of Distances Between Groups

A pair correlation function can be used to determine the distribution of distances between groups by calculating the average number of groups on molecule i that are at a distance r from groups on molecule j.

$$P(r) = \frac{\sum_i \sum_j N_{ij}(r)}{N(N-1)} \qquad (5.9)$$

These distributions for pairs of heads and tails are shown in figures 5.5 and 5.6 respectively. The results are the same for all runs. The distributions in figure 5.5 have
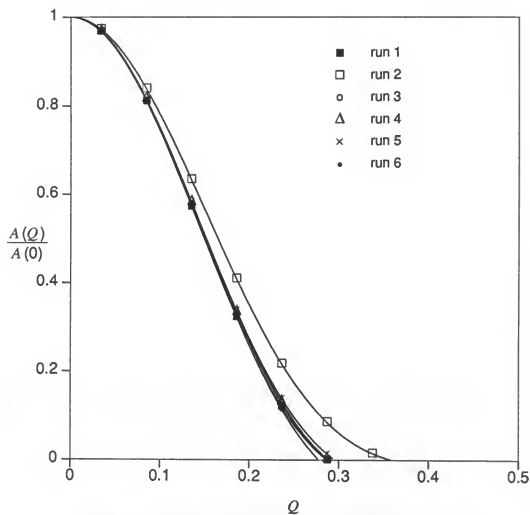
Figure 5.4: Scattering amplitude for methyl tail groups.
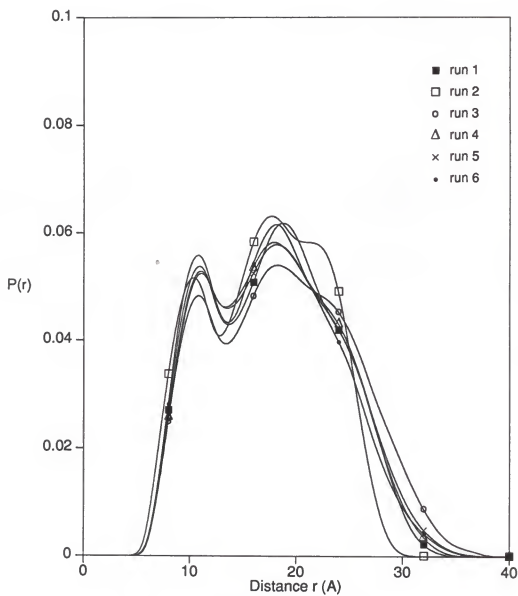
Figure 5.5: Distribution of distances between head groups
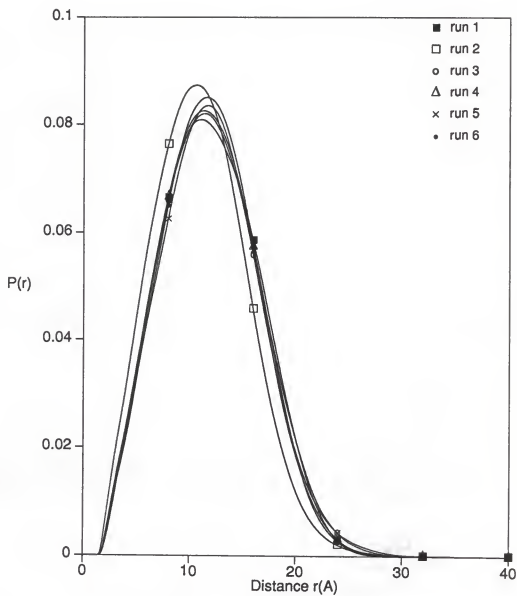
Figure 5.6: Distribution of distances between tail groups

two peaks. The first peak is associated with the pair potential and is due to excluded volume effects, while the second peak is from a reasonably uniform distribution of heads around the micelle surface.

The distributions of distances between tail groups are similar for all runs except run 2. The distribution of distances between tails in run 2 exhibits a peak shifted towards smaller distances. It is probably due to the strong head group harmonic potential keeping the head on the surface of the micelle and forcing all segments into the core. This forces the tail groups into a smaller volume than in other runs.

Micelle Shape

The shape of micelle models can be determined from the principal moments of inertia. We used the ratio of the largest moment of inertia to the smallest moment of inertia where a sphere has a value of unity. A good measure of shape fluctuation is the standard deviation of this ratio. In Figures 5.7 and 5.8, a plot is given of this ratio as a function of time. It can be noted that, to the degree it exists, the period of fluctuations for runs 1 and 2 are somewhat smaller ($\sim$ 3 ps) than for runs 4, 5 and 6 ($\sim$ 10 ps). The presence of the harmonic potential greatly affects the micelle shape by keeping head groups a short distance from the micelle surface. The head–solvent potential has a significant effect on the instantaneous micellar shape.

In table 5.3, average values are listed with their corresponding standard deviations. The results show that, on the average, the micellar shape is slightly non–spherical (ratio $\simeq$ 1.3) except in run 3 (half–harmonic) in which the shape is highly non–
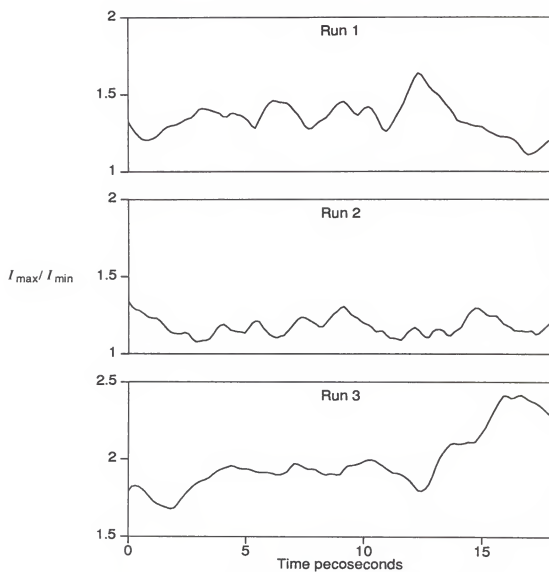
Figure 5.7: Ratio of moments of inertia from runs 1, 2 and 3.
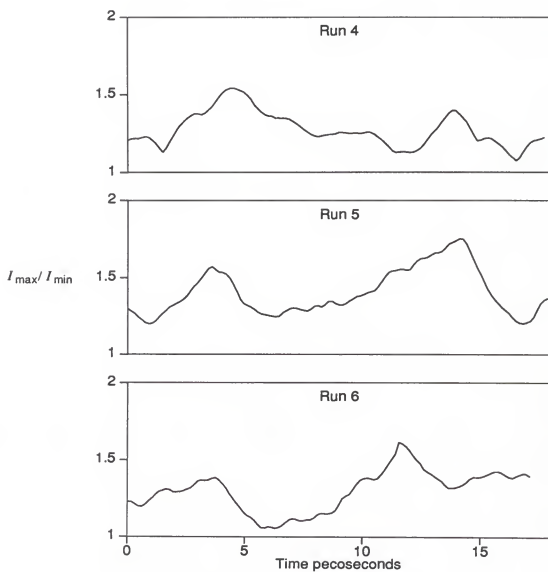
Figure 5.8: Ratio of moments of inertia from runs 4, 5 and 6.

Table 5.3: Average Trans Fraction and Average Ratio of Moments of Inertia

Run	run 1	run 2	run 3	run 4	run 5	run 6
% Trans	59 ± 2	64 ± 2	69 ± 2	63 ± 1	69 ± 4	66 ± 2
I_{max}/I_{min}	1.3 ± 0.1	1.2 ± 0.1	2.0 ± 0.2	1.3 ± 0.1	1.4 ± 0.1	1.3 ± 0.1

spherical (ratio $\simeq 2.0$). The shape fluctuations are not very large ($\sigma \simeq 0.1$) except for run 3 ($\sigma \simeq 0.2$). The different results from run 3 are caused by the half–harmonic head group potential which puts a high energetic wall on head groups from the micellar side, while allowing the head groups to move freely away from the micelle surface. The kinetic effect of the head group movements seems to create stronger shape fluctuations of the micelle.

Chain Conformation. Trans Bond Distributions

A 9–member chain has 6 dihedral angles. A bond is considered to be in a trans position whenever $cos\phi \leq -0.5$ where ϕ is the dihedral angle. Table 5.3 gives the average value of the trans fraction. This value is similar for all runs (67% or about 2 out of 3 bonds are in trans conformation). A similar value was found before for micelles of longer chains (Woods et al., 1986), as well as for octyl micelles with smaller head groups (see Chapter 5) and single chains of various lengths in nonpolar media (see Chapter 2).

Table 5.4 presents the average probability of finding a given number of trans bonds on a chain. The uncertainties may be as large as 0.1. Four out of the six simulations consistently show a most probable value of 4 trans out of 6 bonds. In runs 3 and 6, the most probable value is 5. The probability of finding a chain in total gauche conformation is always zero, while the probability of finding a chain in total trans conformation is small. The distribution among numbers of bonds varies significantly among the runs. In particular, the distribution of run 3 is quite sharp while that

Table 5.4: Probability of a Given Number of Trans Bonds on One Chain

no. of trans bonds	run 1	run 2	run 3	run 4	run 5	run 6
0	0.00	0.00	0.00	0.00	0.00	0.00
1	0.04	0.01	0.01	0.02	0.01	0.05
2	0.13	0.09	0.06	0.11	0.08	0.30
3	0.28	0.28	0.22	0.26	0.18	0.28
4	0.37	0.32	0.25	0.35	0.32	0.23
5	0.16	0.26	0.41	0.20	0.29	0.33
6	0.02	0.05	0.05	0.07	0.12	0.07
$-\sum p_i ln p_i$	1.49	1.48	1.41	1.55	1.53	1.76

of run 6 is quite broad. Entropy values calculated from $S/R = -\sum P_i ln P_i$ are also given in table 5.4 and appear to be similar, though run 3 is smaller while run 6 is much larger.

Table 5.5 presents the probabilities of finding a particular bond on the chain in the trans conformation. Results from five out of six simulations show that bond number 2 (dihedral angle involving groups 1–4) has the highest probability among all bonds to be in trans conformation with the others being about equal. This probably arises from the different bond and head group potential models. Run 1 appears to be different, perhaps due to poorer statistics.

<u>Bond Orientation</u>

An indicator of the chain conformation is the overall bond order parameter, $S(r)$, defined by:

$$S(r) = < \frac{1}{2}(3\cos^2\theta - 1) > \tag{5.10}$$

where θ is the angle formed by the bond vector connecting two adjacent groups and the radius vector from the aggregate center of mass to the center of the bond. Figures 5.9 and 5.10 show that for all runs the overall bond parameter is positive, reaching a high preferential ordering at the micelle surface and a somewhat preferential ordering at the micelle center.

Individual bond order parameters S_i can be calculated for each bond on the chain

$$S_i = < \frac{1}{2}\left(3\cos^2\theta_i - 1\right) > \tag{5.11}$$

Table 5.5: Probability of a Particular Bond Being Trans.

bond no.	run 1	run 2	run 3	run 4	run 5	run 6
2	0.14	0.24	0.20	0.23	0.21	0.20
3	0.20	0.16	0.15	0.15	0.16	0.14
4	0.18	0.17	0.13	0.15	0.16	0.18
5	0.18	0.13	0.17	0.15	0.15	0.16
6	0.17	0.17	0.16	0.20	0.15	0.18
7	0.14	0.14	0.20	0.13	0.17	0.13
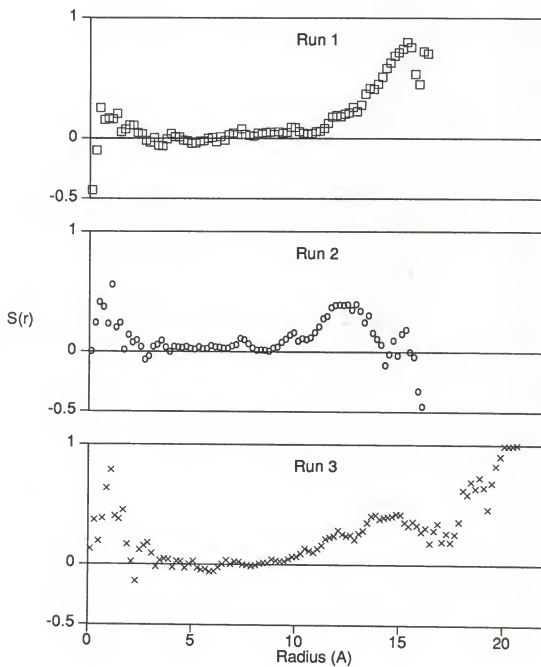
Figure 5.9: Overall bond order parameter $S(r)$ throughout the micelle for runs 1, 2 and 3.
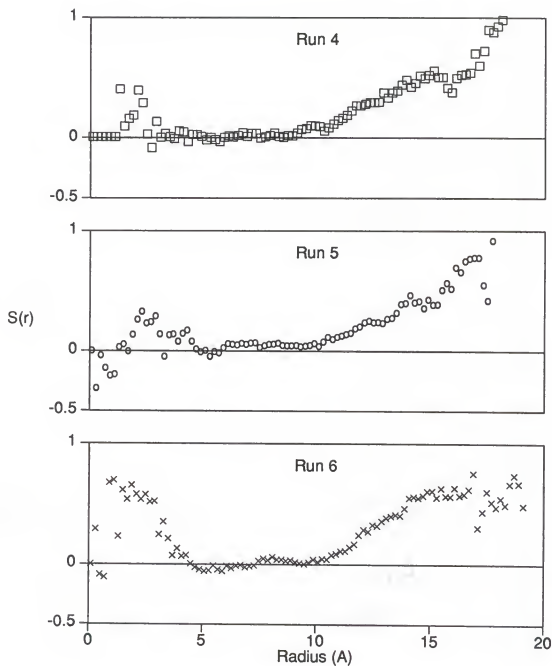
Figure 5.10: Overall bond order parameter $S(r)$ throughout the micelle for runs 4, 5 and 6.

where θ_i is the angle formed by a bond vector between segment centers and the radius vector from the aggregate center of mass to the bond center. Figure 5.11 shows that the individual bond order parameters from all six runs are very similar.

The bond between the head group and the first segment shows the most preferential ordering, generally normal to the micelle surface, but the other bonds on the chain show little preferred order.

Conclusions

Six molecular dynamics simulations have been made to study the effects of different interaction models between micelles and their environment. In general, core structure results are insensitive to different forms. There are some effects on head group distributions, but few differences appear for segments along the chain.

While the head distributions differ among the runs, all show movement of heads into the core. This is probably caused by excluded volume effects at the surface when the head groups are larger than the segments. The excluded volume effect is also seen in the pair correlations between head groups.

The average radial positions of the segments are generally similar. In all runs the average tail group position is further from the center than the adjacent segments, implying some curled chain conformation.

Micellar shape is generally nonspherical to some degree even though the force field representing the micelle–environment interactions is spherical.
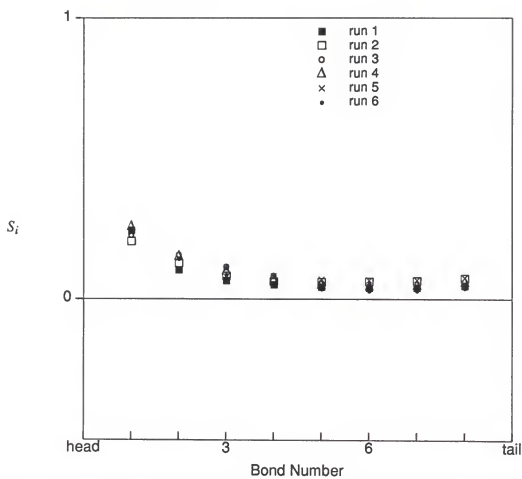
Figure 5.11: Individual bond order parameter S_i for bonds on the 9–member chains from runs 1–6.

The chain conformation results show great similarity among the runs with an average trans fraction of 67% and chains are never in a completely gauche conformation. The first bond on the chain tends to have the highest probability among all bonds to be in trans conformation, and is usually the most preferentially ordered among the bonds.

CHAPTER 6
EFFECTS OF CHAIN LENGTH AND HEAD GROUP CHARACTERISTICS

In the previous chapters, molecular dynamics simulations were used to determine the effect of micelle–solvent models on the micelle behavior. In this chapter we turn to the effect of chain length and head group properties on the internal micelle structure, micellar shape and chain conformation inside the micelle. The results from one molecular dynamics simulation of a octyl "polar methyl" micelle and one of a nonane hydrocarbon droplet are compared with an octyl "nonionic sulfate" micelle from the previous chapter (Run 5) and the dodecyl "polar methyl" micelle described by Woods et al. (1986)

Local structure

One primary measure of micellar molecular structure is the set of spatial probability distributions of the chain segments. A convenient form to use is $r^2 \rho_i(r)$ versus r, which is within a multiplicative constant of the true probability, $P_i(r)$ (see section 5.1). This particular form yields an equal area under the curves for all segments in all runs, and so is a good basis for comparison. When comparing runs with different aggregation numbers a suitable scaling for the micelle radius or any other distance is the ratio of the aggregate numbers to the one–third power. This scaling procedure

seems appropriate because the micelle volume is proportional to the aggregation number.

Results for the tail group distributions for the hydrocarbon droplet (run 8) are shown in figure 6.1. This plot must show symmetry for both ends of the chain; any discrepancy gives a measure of uncertainty in the distributions. The figure indicates that the agreement is excellent at large and small values of r, and small differences appear at the peak.

Results for the tail group distributions for runs 5, 7 and 8, are shown in figure 6.2 along with the results from a micelle with 24 octyl "polar methyl" heads (Farrell, 1988) and a micelle with 52 dodecyl "polar methyl" heads (Woods et al., 1986). Both simulations have an infinite wall chain–solvent interaction model (Equation 4.4) and a harmonic potential head–solvent interaction model (Equation 4.6). The micelle radius for Woods et al. (1986) has been scaled by the $(N/N_1)^{1/3}$ to account for the difference in aggregate numbers ($N = 24$ for runs 5, 7 and 8 and for Farrell, and $N_1 = 52$ for Woods et al.), and the distribution is normalized. The curves for all systems appear statistically different though the most important feature is that tail groups are found everywhere in the micelle in all cases. On the other hand it is difficult to separate the effects of chain length, head size and chain-solvent interaction model. It appears that the only major difference is that the broad distributions of the small heads (runs 7, Woods et al. (1986) and Farrell (1988)) can be distinguished from the sharper "nonionic sulfate" (run 5) and hydrocarbon droplet (run 8) results. The latter are
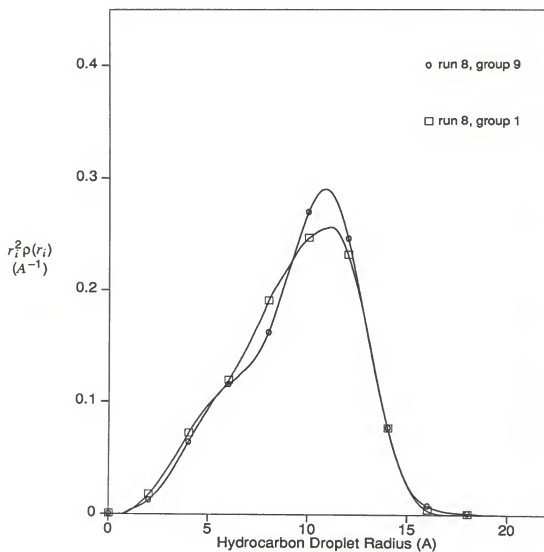
Figure 6.1: Group probability distributions of chain ends of a model hydrocarbon droplet.
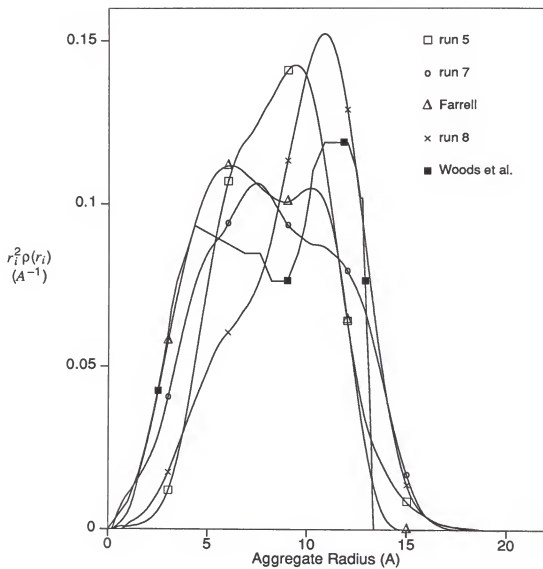
Figure 6.2: Group probability distributions of tails for systems 5, 7 and 8, and from Woods et al. (1986). The distribution by Woods et al. is scaled by $(24/52)^{1/3}$.

due to head groups excluding tails from the palisade region in the first case and the tendency of tails to collect at the interface in the second.

To test whether the results of our solvent field models are consistent with full simulations having solvent molecules, figure 6.3 compares scaled tail distributions from our run 5 with those of Watanabe et al. (1988) and of Jönsson et al. (RC model) (1986). The micelle radius is scaled by $(1/N)^{1/3}$ to account for the difference in aggregate numbers ($N = 24$ for run 5 and $N = 15$ for Watanabe et al. and Jönsson et al.) The agreement is excellent.

The head group distributions of the micelles are shown in figure 6.4 where the scaling by $(N/N_1)^{1/3}$ is used on the results from Woods et al. (1986). The head group distribution is sharp for the smaller head groups, regardless of chain length and interaction whereas larger head groups are broadly distributed with a second peak at the micelle center. As explained in the previous chapter this is an excluded volume effect.

The peak heights of runs 7 and Farrell (1988) (octyl chains) are slightly displaced from those of Woods et al. (1986) (dodecyl chains) even though the head group distribution for the dodecyl "polar methyl" micelle is scaled by the one–third power of the aggregate number ratio, and is normalized to achieve an equal area under all curves. Whether this effect is significant or not is unknown.
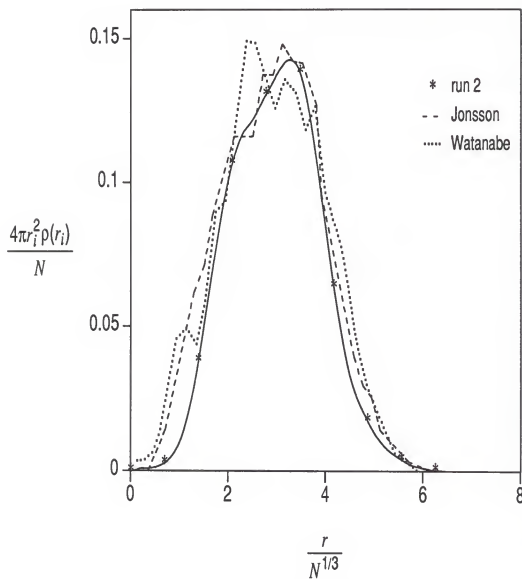
Figure 6.3: Group probability distributions of tails from run 5 and from Watanabe et al. (1988) and Jŏnsson et al. (1986)
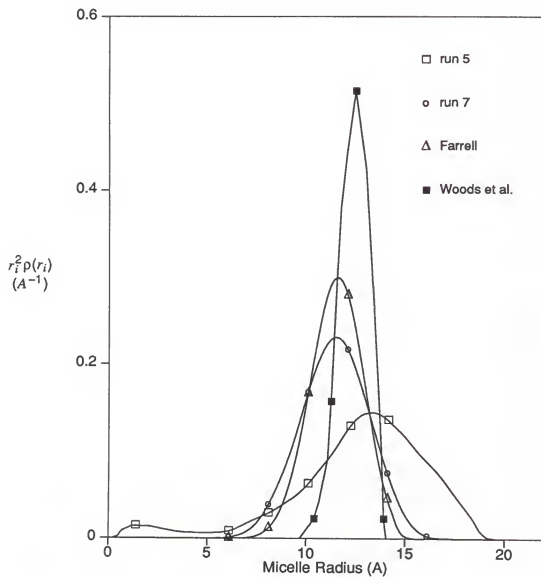
Figure 6.4: Probability distributions of head groups for systems 5 and 7, Farrell (1988) and from Woods et al. (1986). The probability distribution of Woods et al. is scaled by $(24/52)^{1/3}$.

Hydrocarbon distribution

The hydrocarbon distribution is the sum of all chain segment distributions. A plot of this distribution (figure 6.5) shows no significant difference between the octyl micelles and the hydrocarbon droplet. Thus the micelle core structure is essentially that of a hydrocarbon. The scaled and normalized results from Jönsson et al. (1986) show excellent agreement with our results.

Average Chain Segment Positions

Further information on the local structure of groups is given by the average radial position for each group. The results for all simulations are shown in Table 6.1. For run 7, the average position decreases faster closer to the head group and is nearly constant for the last four groups. However, in run 5 the tail group is significantly further from the micelle center than are groups 6, 7 and 8. This appears to be due to the large head group having some tendency to be in the center. The hydrocarbon droplet (run 8) shows significant "backward flux" with tails being at the solvent interface. The required symmetry is shown.

To study the effect of aggregate number and chain length on the average position of groups, a proper basis for comparisons is required. In particular, the tail-to-tail or head-to-head bases are not appropriate. However the chain positions can be treated as continuous variables and average positions can be calculated for the same fractional location on a longer or shorter chain that corresponds to segments in the octyl chain. These positions can be scaled by the one-third power of the ratio
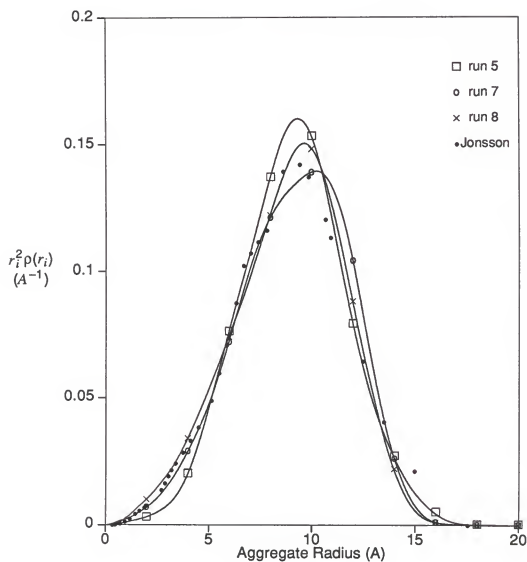
Figure 6.5: Hydrocarbon distributions for runs 5, 7 and 8, and from the micelle simulation of Jönsson et al. (RC model) (1986). The Jönsson distribution is scaled by $(24/15)^{1/3}$.

Table 6.1: Average Radial Position for Each Group After Scaling (See Text), $\bar{R}_i$, (Å) Relative to the Aggregate Center of Mass.

group no	run 5	run 7	run 8	Woods et al. scaled	Jönsson et al. scaled	Watanabe et al. scaled
1	12.5	11.4	9.4	11.9	11.1	14.2
2	10.6	10.8	9.0	11.1	10.4	13.2
3	9.7	10.1	8.6	10.3	9.6	12.2
4	9.2	9.4	8.5	9.5	9.0	11.3
5	8.4	8.9	8.4	8.7	8.5	10.5
6	8.2	8.5	8.5	8.3	8.3	9.8
7	7.9	8.4	8.8	8.0	8.2	9.1
8	8.0	8.2	9.1	8.0	8.2	8.7
9	8.4	8.3	9.6	8.0	8.4	8.3

of aggregate numbers. The result of this comparison is good agreement between the average positions of run 7 and the scaled positions of Woods et al. (1986). (Statistical error of $\pm$ 0.1 Å). Thus the relative effect of chain length on average position is negligible. If similar scaling is used on the average positions reported by Jönsson et al. (1986) and by Watanabe et al. (1988), it can be seen from figure 6.6 that there is excellent agreement between those of Jönsson et al. and the present ones while those from the Watanabe et al. are different, being monotonic and further out. This may be due to a higher trans fraction in the chain that could be an artifact of their simulation that had constrained chain angles (Helfland, 1979; Rallison, 1979). Toxvaerd (1987) has reported that the number of trans–gauche transitions per picosecond decreased from 0.333 to 0.231 when constraints are applied to a decane molecule, resulting in greater trans fractions in shorter runs. The same effect may be present here.

Distributions of tail groups

The tail distribution of figure 6.2 can be compared with measurements of Bendedouch et al. (1983a) using small angle neutron scattering (SANS) on lithium dodecyl sulfate. This system has a head group with similar size and mass to that in run 5 and a chain length similar to that of Woods et al. (1986). The scattering vector Q is scaled with $(N_1/N)^{1/3}$ to account for the difference in aggregation numbers (N_1=78 for Bendedouch et al. (1983a), N_1=52 for Woods et al. and N=24 for runs 5, 7 and 8).
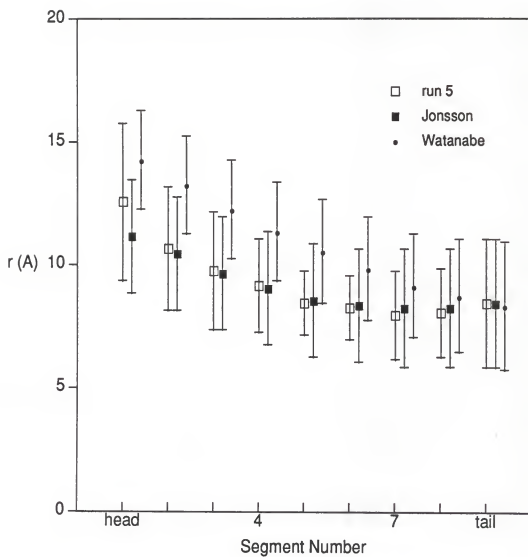
Figure 6.6: Scaled average radial positions for run 5, and from the micelle simulations of Jönsson et al. (RC model) (1986) and of Watanabe et al. (1988).

Figure 6.7 presents the scattering amplitudes for tails, from runs 5, 7 and 8, from Woods et al. (1986) and from Bendedouch et al. (1983a). The results from Bendedouch et al. are truncated at the likely limits suggested by Chevalier and Chachaty (1985). The scattering amplitude plot shows excellent agreement with the results of Woods et al. (1986) and experimental data, and small differences with the results of runs 5 and 7 and experimental data. The fact that figure 6.2 shows such dramatic differences among runs, while figure 6.7 does not, confirms the insensitivity of scattering amplitudes (Cabane et al., 1985; Chevalier and Chachaty, 1985).

Distribution of Distances Between Groups

The distribution of distances between tail groups is shown in Figures 6.8 and 6.9. Figure 6.8 is a test of the symmetry between the chain tails in the hydrocarbon droplet. The difference between the three distributions gives a quantitative idea of the error that would be expected in micelle distributions. In this case it was found to be about 5%.

In figure 6.9 the distributions of distances between tail groups from runs 5, 7 and 8 are compared with the SANS data of Cabane et al. (1985) that was scaled by $(N/N_1)^{1/3}$ to account for the difference in aggregation numbers ($N = 24$ for runs 5, 7 and 8, $N_1 = 74$ for Cabane et al.). The difference between the distributions of runs 5 and 7 and the SANS data is very small. Apparently the head group size does not make much difference. The distributions from the hydrocarbon droplet are also slightly shifted from those of the SANS data, enhancing the idea that the micelle
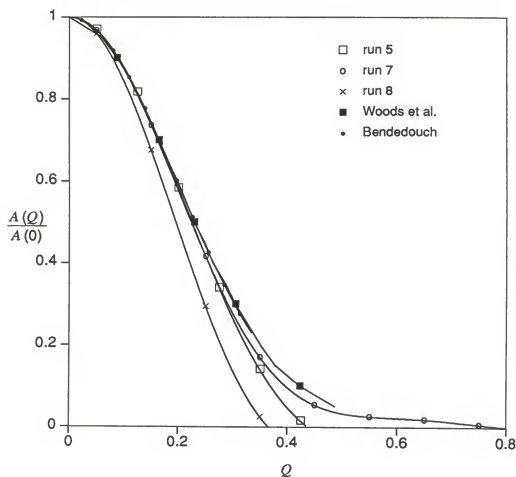
Figure 6.7: Scattering amplitude from methyl tails for runs 5, 7 and 8, from Woods et al. (1986) and from Bendedouch et al. (1983a)
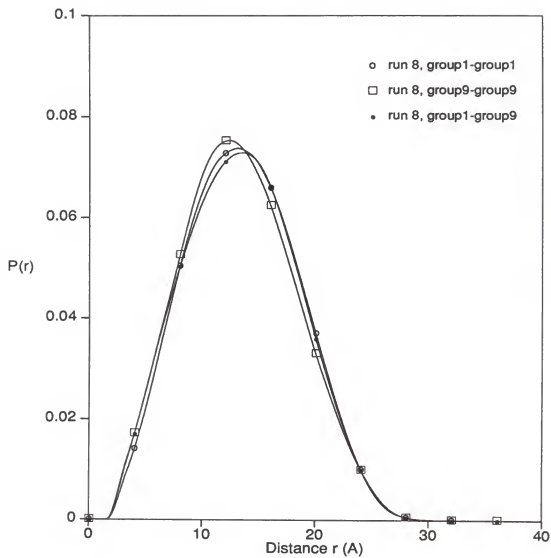
Figure 6.8: Distribution of distances between tail groups of a model hydrocarbon droplet.
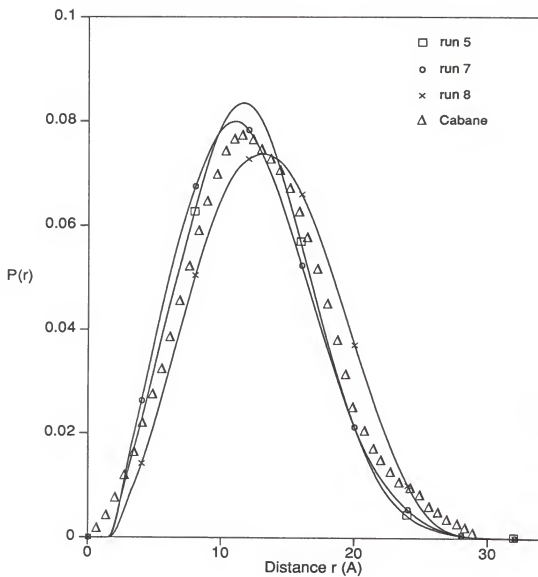
Figure 6.9: Distribution of distances between tail groups as determined from runs 5, 7 and 8 and the SANS data of Cabane et al. (1985). The Cabane distribution is scaled by $(24/74)^{1/3}$.

core is a hydrocarbon–like interior. The level of agreement between these micelle simulations and the tail-tail distributions is different from other models. Cabane et al. (1985) noted that most other models (Fromherz, 1981; Dill and Flory; 1981; Gruen; 1985a) predict too sharp a distribution of distances that is shifted toward smaller distances.

In figure 6.10 the distributions of distances between all groups within the core from runs 5, 7 and 8 are compared with the same SANS data of Cabane et al. (1985). This quantity differs from P in equation 5.9 only in that i ranges over all groups on a molecule and j covers all groups on all other molecules. The denominator is $(l-1)^2 N(N-1)$, where l is the number of groups on a chain. The agreement between the micelle simulations from runs 5 and 7 and the hydrocarbon simulation of run 8 is excellent, indicating no head group size effect on this particular distribution and confirming the hydrocarbon–like core for micelles. The peak positions from our runs are slightly shifted toward smaller distances compared to those of the data, even after using the usual scaling by the aggregation number to the one–third power. This may either suggest that this particular distribution is affected by chain length, or that a different scaling should be used. If the distribution of Cabane et al. (1985) is scaled by the total number of segments instead of the aggregation number, excellent agreement occurs (Figure 6.10).

Figure 6.11 shows that the head group pair distributions in runs 5, 7 and 8 are significantly different. In particular, the head group size affects the distribution since
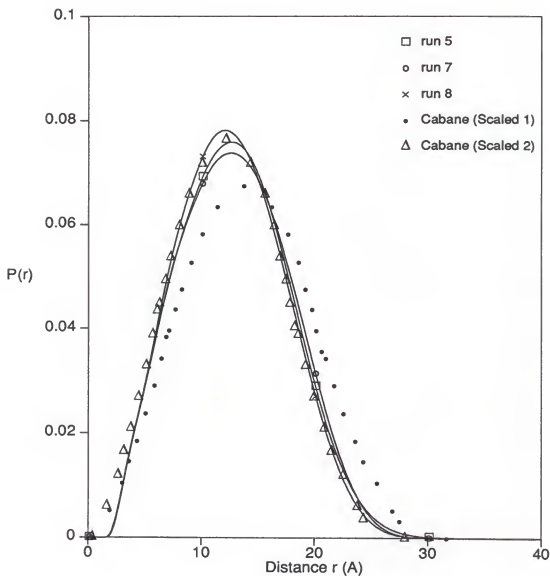
Figure 6.10: Distribution of distances within the whole core as determined from runs 5, 7 and 8 and the scaled SANS data of Cabane et al. (1985). The Cabane (Scaled 1) distribution is scaled by $(24/74)^{1/3}$ and the Cabane (scaled 2) by $(216/962)^{1/3}$.
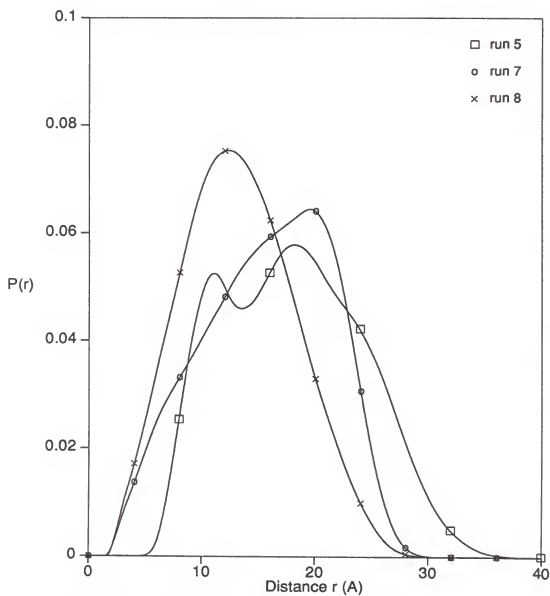
Figure 6.11: Distribution of distances between head groups

two peaks are present in run 5 while only one peak is present in run 7. There is a crowding of the larger head groups around the micelle surface in run 5. The first peak is associated with the pair potential while the second peak (located where the smaller head peak is) is from a reasonably uniform distribution of heads around the micelle interface. The distribution of distances between tails in the hydrocarbon droplet is shown for comparison. As expected, the peak for non surfactant chains occurs at a shorter distance due to their freedom to travel throughout the hydrocarbon droplet.

Micelle Shape

The shape of the model micelles can be indicated by values of the principal moments of inertia. One measure of nonsphericity is the ratio of the largest moment of inertia to the smallest moment of inertia which is unity for a sphere and greater than one for nonspherical shapes. A good measure of shape fluctuations is the standard deviation from the mean of this ratio. In Figure 6.12, a plot is given of this ratio as a function of time. It can be noted that both the period and the amplitude of fluctuations for run 5 are somewhat larger than for runs 7 and 8. Peaks for run 5 are separated by about 10 picoseconds while peaks for runs 7 and 8 are separated by only 5 picoseconds. The harmonic potential for the heads groups in run 7 is responsible for keeping them a short distance from the micelle surface, i.e. the frequency imposed by the harmonic potential controls the period of shape fluctuations. In run 8 the lack of head–solvent interactions results in very small fluctuations about the average aggregate shape because chains can extend only a small fraction of their total lengths

beyond the micelle surface. In table 6.2, the average values of the ratio of moments of inertia maxima are listed with a corresponding standard deviation. The results show that on the average, the micellar shape is slightly non-spherical, and the shape fluctuations are generally small, as from experiment (Hayter, 1981).

Chain Conformation. Trans Bond Distributions

A N–member chain has N–3 dihedral angles. A bond is considered to be in a trans position whenever $cos\phi \leq -0.5$ where ϕ is the dihedral angle. Table 6.2 gives average values of the trans fraction for all systems. The value is essentially the same for all runs (72%). We found a similar value with different rotational potentials (Jorgensen, 1984) in a 24 octyl "polar methyl" micelle. Other micelle simulations have yielded different average trans fractions. Watanabe et al. (1988) reported a value of 78% while Jönsson et al. (1986) reported a value of 50%. As discussed above, the discrepancy between our results and those of Watanabe et al. (1988) could be a result of their chain angle constraints. The origin of the large difference in results from our runs and those of Jönsson et al. (1986) is unknown.

Table 6.3 presents the average probability of finding a given number of trans bonds on one chain, as found from all four simulations. The most probable value in all simulations is 4 out of 6 bonds (7 out of 10 for Woods et al. (1986)), consistent with the average trans fraction. Table 5.4 also shows that the probability of finding a chain in the all gauche conformation is zero.
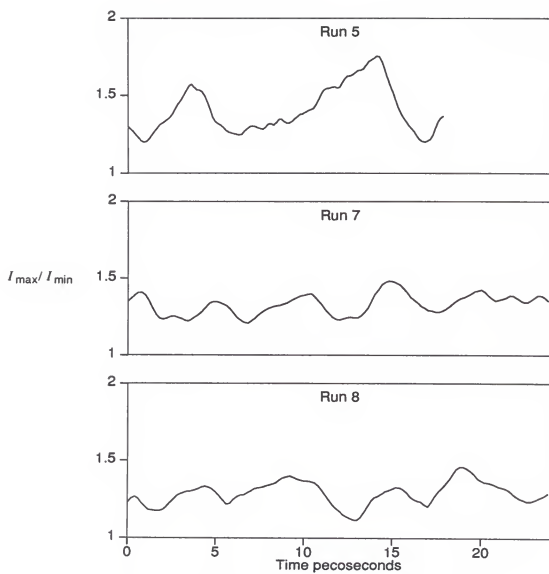
Figure 6.12: Ratio of moments of inertia from runs 5, 7 and 8.

Table 6.2: Average Trans Fraction and Average Ratio of Moments of Inertia

Run	run 5	run 7	run 8	Woods et al.
% Trans	69 ± 4	74 ± 2	70 ± 2	72 ± 3
I_{max}/I_{min}	1.4 ± 0.1	1.4 ± 0.1	1.3 ± 0.1	1.2 ± 0.1

Table 6.3: Probability of Finding a Given Number of Trans Bonds on One Chain

no. of trans bonds	run 5	run 7	run 8	Woods et al.
0	0.00	0.00	0.00	0.00
1	0.01	0.01	0.01	0.00
2	0.08	0.04	0.06	0.00
3	0.18	0.13	0.15	0.00
4	0.32	0.33	0.38	0.02
5	0.29	0.32	0.30	0.09
6	0.12	0.18	0.10	0.17
7				0.30
8				0.27
9				0.12
10				0.03

Table 6.4 presents the probabilities for finding a particular bond on the chain in the trans conformation. Results from simulations 5, 8 and that of Woods et al. (1986) show an essentially flat distribution among all bonds, while run 5 has bond 2 (dihedral angle involving the head and segments 2–4) with a distinctly higher probability to be in the trans conformation. The "nonionic sulfate" mass, size and bond forces apparently affect the first dihedral bond conformation. Chevalier and Chachaty (1985) obtained similar results from NMR measurements. They suggest that the increase is due to micellization, but we believe that it is due to the nature of the head group. A single surfactant molecule with a large head group in a hydrocarbon fluid of methane groups showed the same increase in trans fraction around the head group.

Bond Orientation

An indicator of the chain conformation is the bond order parameter, $S(r)$, defined by:

$$S(r) = <\frac{1}{2}(3\cos^2\theta - 1)> \tag{6.1}$$

where θ is the angle formed by the bond vector connecting two adjacent groups and the radius vector from the aggregate center of mass to the center of the bond. A value of 1 for $S(r)$ indicates that bonds are parallel to the micelle radius, and a value of -0.5 indicates that bonds are normal to the micelle radius, while a value of 0 indicates no preferential ordering. Figure 6.13 shows that for run 5 the bond parameter is positive for $r > 10$ Å indicating an ordering of bonds parallel to the micelle radius, while for

Table 6.4: Probability of Finding a Particular Bond in the Trans Conformation

bond no.	run 5	run 7	run 8	Woods et al.
2	0.21	0.16	0.15	0.09
3	0.16	0.17	0.15	0.08
4	0.16	0.16	0.17	0.10
5	0.15	0.18	0.15	0.09
6	0.15	0.18	0.18	0.09
7	0.17	0.15	0.18	0.13
8				0.10
9				0.11
10				0.09
11				0.12
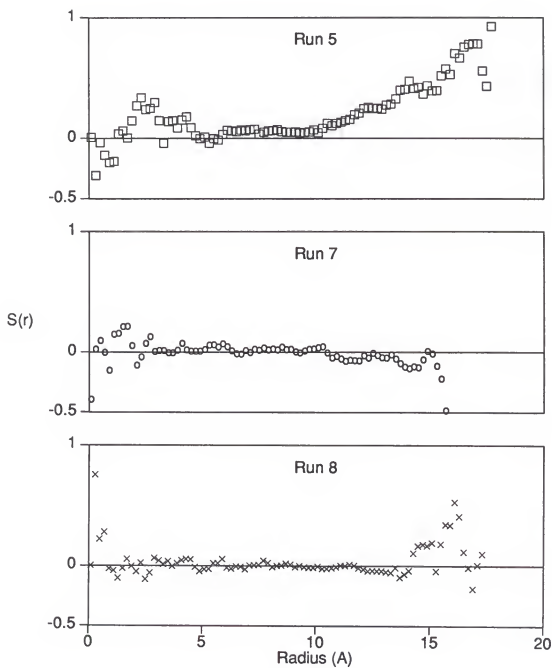
Figure 6.13: Bond order parameter $S(r)$ throughout the micelle, for runs 5, 7 and 8.

runs 7 and 8 the bond parameter is zero except at the surface and the center. The scatter in the values at very small and very large r seen in the figure is a consequence of the relatively small number of bonds to be sampled there. The preferential ordering of run 5 is due to excluded volume effects since head groups totally occupy the micelle surface forcing the first few bonds to be parallel to the micelle radius.

Another indicator of chain conformation is the bond order parameter S_i which can be calculated for each bond, i, on the chain from

$$S_i = < (1/2) \left(3cos^2\theta_i - 1 \right) > \tag{6.2}$$

where θ_i is the angle formed by the bond vector connecting the adjacent segment centers and the radius vector from the aggregate center of mass to the center of the bond. Figure 6.14 shows that for runs 7 and 8, the bonds in the chain show no preferred order, while for run 5 the bond between the head group and the first segment shows the most preferential ordering, and bonds along the chain show less, but finite, preferred order. The latter is consistent with the first dihedral bond having a higher fraction of trans conformation and the segments being excluded from the surface. In Woods et al. (1986) all bonds have a positive order parameter, suggesting a slight preference of bonds to be parallel to the micelle radius. This arises from the infinite wall chain–solvent interaction model used in their model tending to keep segments from reaching the micelle surface. The finite barrier potential of runs 7 and 8 does not exhibit any order.
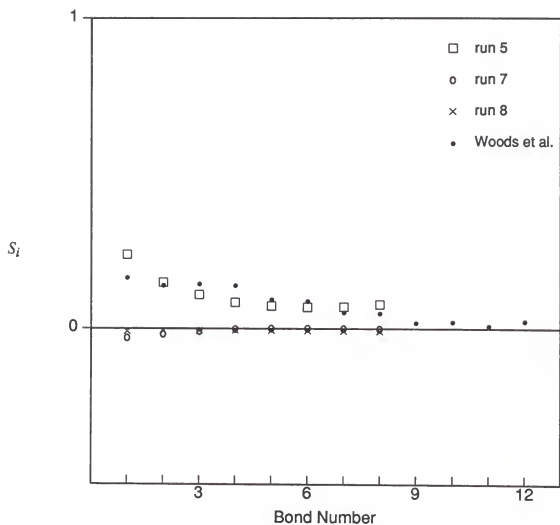
Figure 6.14: Bond order parameter S_i for individual bonds on the N–member chains for runs 5, 7 and 8 and from Woods et al. (1986).

Conclusions

The results from several molecular dynamics simulations have shown the effects of head group size and chain length on micellar behavior. From simulations of other workers and the present study including comparison with experimental data, several significant conclusions can be drawn concerning micellar interior structure and shape as well as chain conformation.

The results from the total segment distribution indicate a hydrocarbon–like interior in the micelle core. Consistent with SANS data (Cabane et al., 1985), the tail-tail distribution of distances is not like those of all trans conformations nor simplified statistical models which are shifted to smaller distances and are sharper. The average position of segments in the micelle is independent of chain length and head group. It is consistent with other simulation (Jönsson et al., 1986), while tail singlet distributions compare well with two full simulations (Jönsson et al., 1986; Watanabe et al., 1988).

The micelle shape is not affected by chain length or head group size, and on the average is slightly nonspherical with small, but not negligible, shape fluctuations.

The conformation of chains is independent of head group size or chain length. The trans fraction in the chains was found in all runs to be around 72%. This value was found to be independent of rotational potential or intermolecular potential.

CHAPTER 7
CONCLUSIONS AND RECOMMENDATIONS

Molecular dynamics methods have been used to study micellar structure, and alkane and surfactant conformation in dilute solutions. A summary of the most important conclusions that have been reached during the course of this study are listed in this chapter.

In general, n-alkanes in a monatomic fluid of methylene segments were found to have the same trans fraction independent of chain length, while other properties such as radius of gyration and end–to–end distance are linear with chain length. From the simulations of surfactant molecules, it is apparent that ionic surfactants behave differently in a nonpolar fluid than in water.

The conformation of ionic surfactants in nonpolar fluids was found to be similar to that of n-alkanes in the same fluids, but the average trans fraction of these surfactants was found to be significantly smaller in water than in a monatomic fluid of segments.

The general results from the micelle simulations indicate that structural results are insensitive to different micelle–solvent interaction models, although there are noticeable effects on head group distributions. Simulation results show movements of heads into the core that could be best explained by an excluded volume effect at the micellar surface resulting from the large size of these head groups. Surfactant chains in micelles are not in the all–trans conformation but are curled toward the

surface. On average, the tail group position is further from the micelle center than the adjacent segments. Analysis of moment of inertia shows that micellar shape is on the average somewhat nonspherical, and is strongly affected by the nature of the head group–solvent interaction model.

Analysis from micelle and hydrocarbon droplet simulations with different chain lengths and head sizes shows that properties such as average radial positions of segments, micellar shapes and chain conformations are not affected by the size of the head group or the length of the chain, while other properties such as singlet radial distributions and distributions of distances between segments do depend on the surfactant characteristics.

In general, results from all micelle simulations indicate that the micellar core is hydrocarbon like, and that the conformation of micellar surfactants is much like that of ionic surfactants in nonpolar fluids.

The results found here have been generally consistent with experiment and other simulations yielding a consistant understanding about micellar structure. Nonetheless, to fully understand the process of micelle formation future research should examine in more details the conformation of ionic and nonionic surfactants prior to micellization, and study the structure of water in the presence of these surfactants.

The micelle model that has been originally developed by Woods et al. (1985) and improved in this study might be usable to study the solubilization of nonpolar species in micellar solutions and to investigate the catalytic capabilities of micelles.

The effective solvent environment intermolecular potentials may be pertinent to all surfactant solutions for application to reverse micelles, microemulsions and polymer–surfactant mixtures.

APPENDIX

WATER STRUCTURE IN THE PRESENCE OF AN "ANIONIC METHYL"
SURFACTANT

A.1 Background

Since the advent of molecular dynamics there have been numerous simulations

to study the structure of water in the presence of a solute given a reliable effective

water pair potential. Polar (Rao and Berne, 1981) and nonpolar solutes (Geiger et

al., 1979; Okazaki et al., 1981; Rappaport and Scherega, 1982; Remerie et al., 1984;

Jorgensen et al., 1985; Zichi and Rossky, 1986b; Watanabe and Andersen, 1986;

Tanaka, 1987) have received equal emphasis in simulations due to the importance of

water as a solvent in many applications. While section 3.5 thoroughly analyzed the

conformation of an ionic surfactant in water, this appendix is an in–depth study of

the structure of the water in the presence of the ionic surfactant since surfactants are

a different type of molecules.

Many postulates have been made about the configuration of water molecules

around nonpolar solutes. Most suggest that water molecules around nonpolar so-

lutes form "icebergs" (Frank and Evans, 1945; Nemethy and Scheraga, 1962) or

clathrate–like environments (Glew, 1962) around the inert solute, but there seem

to be no experiments that have strongly supported this picture. Only NMR studies

have showed a slowing of molecular motions around the nonpolar solute (Goldammer and Hertz, 1970).

This analysis is intended to show what simulations indicate about this issue. The model and simulation details for the present study are those described in section 3.5.

A.2 Results and Discussion

Hydration Numbers. The computed primary coordination numbers for the octyl "anionic methyl" surfactant are listed in Table A.1. Coordination numbers for nonspherical solutes can be computed according to the definition of Mehrotra and Beveridge (1980) and Jorgensen et al. (1985) which requires a cutoff distance of 5.35 Å between CH_n groups and water molecules. This value corresponds to the location of the first minimum in the C–O radial distribution functions of methane and other alkanes in water at 25 °C. Water molecules that are within the cutoff distance of two or more surfactant segments are counted towards the coordination number of the nearest segment. The total coordination number of the surfactant molecule is the sum of all segment coordination numbers.

The average coordination numbers are shown in Table A.1 for successive periods in the simulations and for the whole duration. The coordination numbers of the head group and the chain end are much higher than those of the interior segments. In fact the coordination number of the ionic head group (12.46) is about three times higher than for any interior segment, while the tail group coordination number (9.88) is more than a factor of two greater. The difference in the coordination numbers of

Table A.1: Computed Coordination Numbers for an Octyl "Anionic Methyl" Surfactant in Water.

Segment	1	2	3	4	5	6	7	8	9	Total
Period 1	12.21	4.01	3.30	2.99	3.31	2.75	3.20	5.41	9.04	46.22
Period 2	12.29	3.46	3.72	2.29	3.58	3.47	2.64	5.31	9.49	46.27
Period 3	12.56	3.92	3.79	3.12	3.11	3.44	3.40	4.16	9.50	47.00
Period 4	12.04	4.15	3.82	3.24	3.21	2.63	3.28	4.92	10.62	47.90
Period 5	13.17	4.13	2.76	3.51	3.26	2.89	3.69	3.90	10.72	48.03
Average	12.46	3.94	3.48	3.03	3.29	3.04	3.24	4.74	9.88	47.09
Std. Dev.	0.39	0.25	0.41	0.41	0.16	0.35	0.34	0.61	0.67	0.77

end and interior segments is due to the shielding of these segments. Jorgensen et al. (1985) found coordination numbers of 10.7 for the pentane end carbons, 4.7 for the α–carbons and 4.1 for the middle carbon.

The difference in the coordination numbers of the head group and the tail group can be explained by the hydrophilicity of the ionic head group. In fact, this difference would have been much larger without the presence of a counterion which is coupled with with the anionic head group most of the time.

The total coordination number (47.09) is slightly larger than the coordination number of n-nonane (46.00) obtained by extrapolation of the coordination numbers for ethane, propane, butane and pentane as calculated by Jorgensen et al. (1985).

Orientational Structure. Figure A.1 shows the distribution of water dipole vector orientations with respect to segment–water center–to–center vectors for all water molecules present within one cutoff distance of the surfactant molecule. The relative orientation of these vectors are calculated by computing the cosine between the above mentioned vectors.

$$\cos(\alpha) = \hat{u}_{dipole} \cdot \hat{u}_{OS} \tag{A.1}$$

where $\hat{u}_{dipole}$ is the unit vector for the water dipole moment such that:

$$\hat{u}_{dipole} = \frac{\sum_i q_i \vec{r}_i}{|\sum_i q_i \vec{r}_i|} \tag{A.2}$$

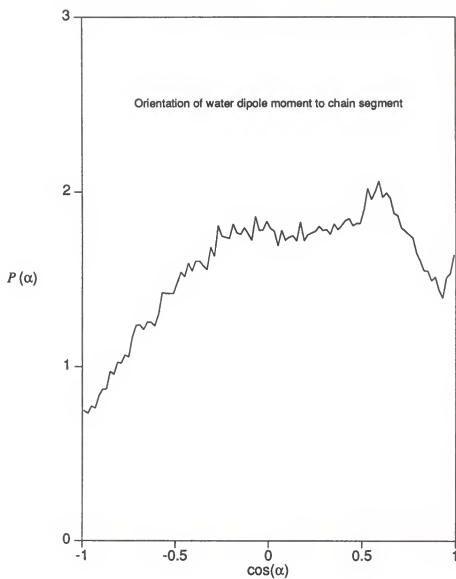and the summation over i is over the atoms in the water molecule. $\hat{u}_{OS}$ is the segment–

Figure A.1: Distribution function for the angle cosines describing the orientation of the water molecule dipole moment with respect to the segment–oxygen vector.

water oxygen unit vector such that:

$$\hat{u}_{OS} = \frac{\vec{r}_O - \vec{r}_S}{|\vec{r}_O - \vec{r}_S|} \qquad (A.3)$$

The cutoff distance $|\vec{r}_O - \vec{r}_S| = 5.35$ Å.

The distribution results show a pronounced preference for positive values of $\cos(\alpha)$. In other words, orientations where both hydrogens of the water are pointing towards the segment $(\cos(\alpha) = -1)$ are avoided, and while those where both hydrogens are partially pointing away $(\cos(\alpha) = 0.6)$ are favored. Similar results were previously found by Geiger et al. (1979) in their study of the hydration of a pair of Lennard–Jones solutes.

Water–Water Radial Pair Correlation Functions. Water–water correlation functions are calculated on a atom–atom basis near the surfactant molecule and in the bulk. As before, water molecules are considered to be in the shell if they are below a cutoff distance of 5.35 Å from the surfactant molecule. All other molecules are considered to be in the bulk. In cases where one water molecule is in the shell and another in the bulk, the atomic distances arising from such a pair contribute to both the shell and the bulk pair correlations.

Figures A.2, A.3 and A.4 show the radial distributions of oxygen–oxygen, hydrogen–hydrogen and oxygen–hydrogen distances in the shell and in the bulk. All distributions show great similarity between the bulk and the shell with the peaks not shifted but only having different magnitudes. This is consistent with the results found by Geiger et al. (1979) that show no discernible shift in peak position but only a dif-
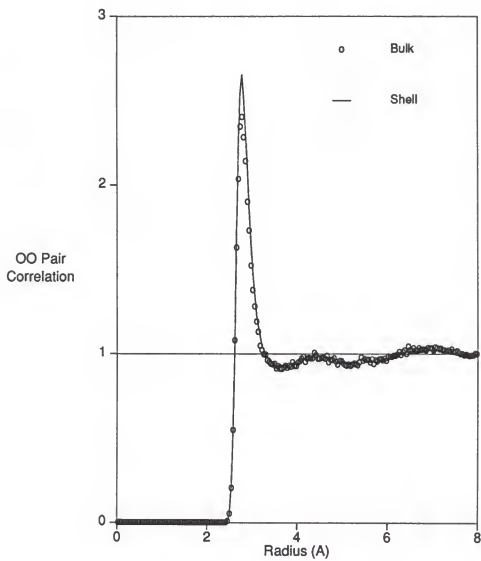
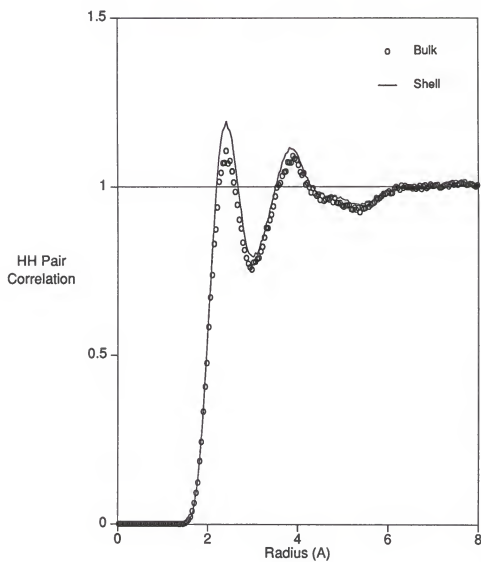Figure A.2: Intermolecular oxygen–oxygen pair correlations function.

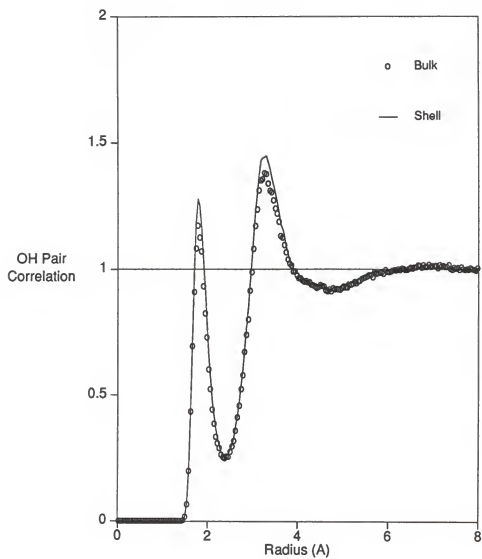Figure A.3: Intermolecular hydrogen–hydrogen pair correlation function.

Figure A.4: Intermolecular oxygen–hydrogen pair correlation functions.

ference in magnitude between the shell and the bulk. In this analysis the peak of the shell distribution is consistently higher than that of the bulk distribution. This indicates a slight structure enhancement in the shell over the bulk. To measure the degree of structure, a ratio of the heights of the first maximum and the following minimum is calculated. Table A.2 shows that this ratio is always higher by a factor of 1.03 to 1.1 for the shell over the bulk. This is not a very large effect. Geiger et al. (1979) have found that the shell–bulk enhancement factor varies from 1.3 to 1.57, but with a shell that is smaller than the one used in this analysis. (Geiger et al. used a shell of 4.5 Å radius).

Water-Surfactant radial pair correlation functions. The water–surfactant pair correlations can be calculated on a segment–to–segment basis. In particular, the oxygen–chain segment, oxygen–head group, hydrogen–chain segment and the hydrogen–head group pair correlation functions have been found. In Figure A.5 the hydrogen–head group distribution is plotted. The first peak at r=1.82 Å has a magnitude of 5.21 and the second peak at r=3.3 Å has a magnitude of 1.89. The first minimum is at r=2.64 Å and has a magnitude of 0.29. The large difference in heights of the first peak and the following minimum indicates a high degree of structure of hydrogen atoms around the head group, as expected from their opposite charges.

Figure A.6 shows the oxygen–head group pair correlation function. This distribution has a very high first peak (magnitude of 4.81) at r=2.82 Å, but a very small second peak (magnitude of 1.20) at r=5.00 Å. The first minimum is at r=3.54 Å and

Table A.2: Ratios of the Heights of the First Maximum and the Following Minimum for Various Water–Water Pair Correlation Functions in Bulk and Shell.

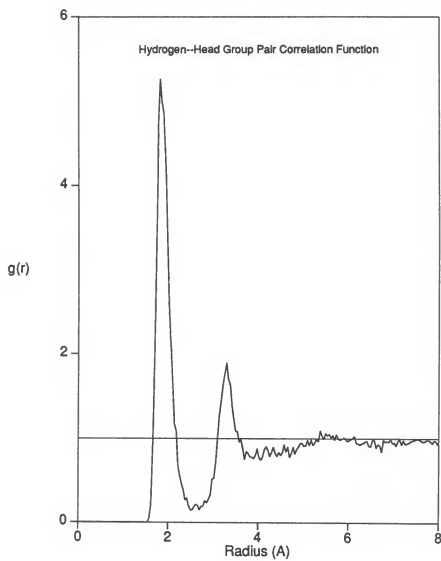|		g_{max}	g_{min}	$\frac{g_{max}}{g_{min}}$	enhancement
g_{OO}	Shell	2.65	0.91	2.91	1.10
	bulk	2.40	0.91	2.64	
g_{OH}	Shell	1.28	0.26	4.92	1.05
	Bulk	1.17	0.25	4.68	
g_{HH}	Shell	1.19	0.79	1.51	1.03
	Bulk	1.11	0.76	1.46	

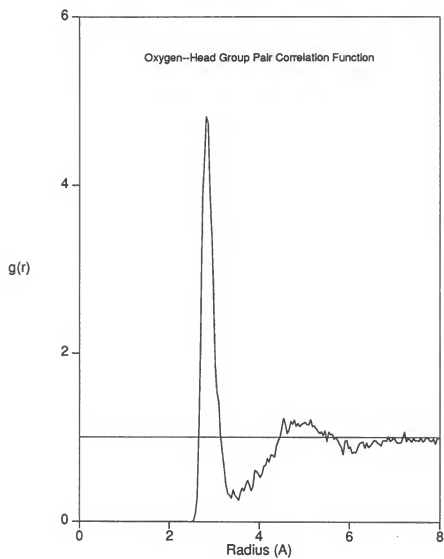Figure A.5: Intermolecular hydrogen–head group pair correlation function.

Figure A.6: Intermolecular oxygen–head group pair correlation functions.

has a magnitude of 0.25. The first peak in the oxygen–head group distribution occurs about 1 Å further away from the head group than the first peak in the hydrogen–head group distribution as expected from the intratomic distance between the oxygen and hydrogen. Thus, oxygen atoms are at the maximum distance away from the head group given that the positively charged hydrogen is strongly attracted to the head group while the negatively charged oxygen atom is strongly repelled. The arrangement of water molecules around the head group is such that only one hydrogen from each water molecule is next to the head group. The distance of the the other hydrogen to the head group is associated with the second peak in the hydrogen–head group distribution.

The hydrogen–chain segment and the oxygen–chain segment distributions are shown in Figures A.7 and A.8. Both distributions show little structure of water molecules around the chain segments. The peak for the hydrogen–chain segment distribution occurs at a much larger distance than the peak for the oxygen–chain segment distribution, confirming that hydrogen atoms tend to point outward from the chain segments.

Self Diffusion. The most significant measure of water dynamics around the surfactant molecule and in the bulk is water self diffusion. The self-diffusion coefficient can be determined by the long time slope of the mean square displacement. Since the present simulation is of the order of 20 picoseconds, calculating an accurate self diffusion is uncertain. However comparisons of the the mean square displacement of
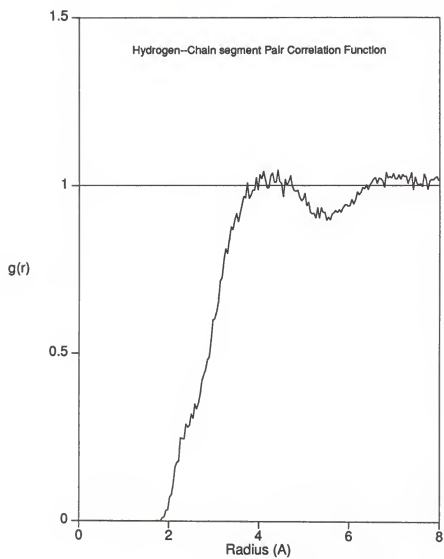
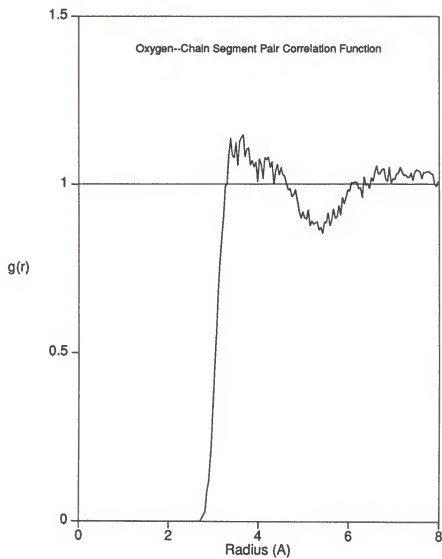Figure A.7: Intermolecular hydrogen–chain segment pair correlation function.

Figure A.8: Intermolecular oxygen–chain segment pair correlation functions.

shell and bulk water can provide a good basis for comparing the motions of both kinds of water molecules.

Since water molecules can move in and out of the shell around the surfactant molecule, separation of the total diffusion of certain molecules into shell or bulk diffusion is difficult. Only those water molecules that are within the shell at time $t = 0$ count towards the shell diffusion, and those which enter the shell after the beginning of the run are not counted. To limit the number of water molecules moving in and out of the shell, the simulation was divided into several small samples of the order of 3 picoseconds, and self diffusion coefficients are calculated only during these small periods. The bulk and shell diffusion coefficients for seven periods are shown in Table A.3. Over the simulation length the results indicate that bulk diffusion is faster than shell diffusion by 14%. Geiger et al. (1979) found a 16% difference.

The results from period 4 are plotted in Figure A.9. The shell and bulk displacement curves have different shapes. The bulk variation is almost linear, but that of the shell is irregular, mainly due to surfactant motions transporting water molecules in the shell.

A.3 Conclusions

Several conclusions can be drawn about the structure and dynamics of water molecules in the proximity of an amphiphilic molecule. It was found that hydration numbers of end segments are much higher than those of the interior segments, and that hydrogen atoms tend to point outward from the nonpolar part of the surfac-

Table A.3: Self–Diffusion coefficients for Bulk and Shell Water Molecules in units of $10^{-5} cm^2/sec$.

Period	1	2	3	4	5	6	7	Total
D_{bulk}	6.9	7.3	6.5	6.9	6.5	6.6	5.3	6.6
D_{shell}	5.4	6.1	5.6	5.7	6.4	5.9	5.4	5.8
$\frac{D_{bulk}}{D_{shell}}$	1.28	1.20	1.16	1.21	1.02	1.12	0.98	1.14

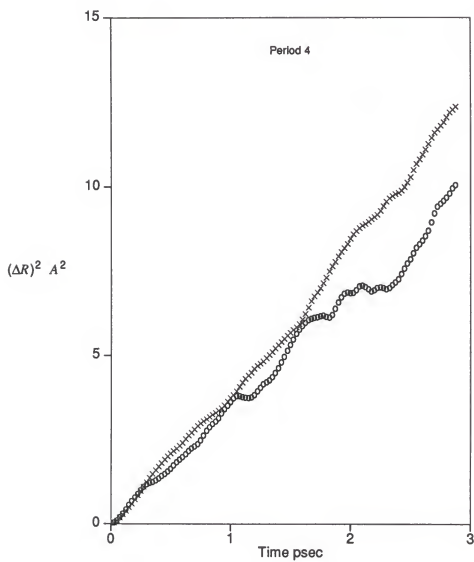Figure A.9: Mean square displacements of water molecules in the shell and the bulk.

tant molecule. Around the surfactant anionic head group only one hydrogen of the water molecule points inward. The water–water pair correlation functions show a slight structure enhancement in the shell over the bulk, while the water self diffusion coefficients are somewhat smaller in the shell than in the bulk.

BIBLIOGRAPHY

Allen, M. P., and D. J. Tildesley, 1987. <u>Computer Simulation of Liquids</u>, Clarendon Press, Oxford.

Alper, H. E., and R. M. Levy, 1989. "Computer Simulations of the Dielectric Properties of Water: Studies of the Simple Point Charge and Transferable Intermolecular Potential Models." Journal of Chemical Physics, $\underline{91}$, 1242

Bañon, A., F. Serrano Adan, and J. Santamaria, 1985. "The Effect of Intermolecular Potential Model on the Structure and Conformational Equilibrium of Liquid n–Butane." Journal of Chemical Physics, $\underline{83}$, 297

Bendedouch, D., S.-H. Chen, and W. C. Koehler, 1983a. "Structure of Ionic Micelles from Small Angle Neutron Scattering." Journal of Physical Chemistry, $\underline{87}$, 153

Bendedouch, D., S.-H. Chen, and W. C. Koehler, 1983b. "Determination of Interparticle Structure Factors in Ionic Micellar Solutions by Small Angle Neutron Scattering." Journal of Physical Chemistry, $\underline{87}$, 2621

Ben–Shaul, A., and W. M. Gelbart, 1985. "Theory of Chain Packing in Amphiphilic Aggregates." Annual Review of Physical Chemistry, $\underline{36}$, 179

Berendsen, H. J. C., J. P. M. Postma, W. F. Van Gunsteren, and J. Hermans, 1981. "Interaction Models for Water in Relation to Protein Hydration." In <u>Intermolecular Forces</u>, B. Pullman ed.; Reidel, Dordrecht, Holland

Bernal, J. D., and R. H. Fowler, 1933. "A Theory of Water, and Ionic Solution, with Particular Reference to Hydrogen and Hydroxyl Ions." Journal of Chemical Physics, $\underline{1}$, 515

Bigot, B., and W. L. Jorgensen, 1981. "Sampling Methods for Monte Carlo Simulations of n–Butane in Dilute Solution." Journal of Chemical Physics, $\underline{75}$, 1944

Cabane, B., 1981. "Structure of the Water/Surfactant Interface in Micelles: An NMR Study of SDS Micelles Labeled with Paramagnetic Ions." Journal de Physique, $\underline{42}$, 847

156

Cabane, B., 1987. "Small Angle Neutron Scattering." In Surfactant Solutions, New Methods of Investigation; Raoul Zana ed.; Dekker, New York

Cabane, B., R. Duplessix, and T. Zemb, 1985. "High Resolution Neutron Scattering on Ionic Surfactant Micelles: SDS in Water." Journal de Physique, 46, 133

Candau, J., 1987. "Light Scattering." In Surfactant Solutions, New Methods of Investigation; Raoul Zana ed.; Dekker, New York

Cantor, R. S., and K. A. Dill, 1984. "Statistical Thermodynamics of Short Chain Molecule Interphases 2. Configurational Properties of Amphiphilic Aggregates." Macromolecules, 17, 380

Chang, N. J., and E. W. Kaler, 1985. "The Structure of Sodium Dodecyl Sulfate Micelles in Solutions of H_2O and D_2O." Journal of Physical Chemistry, 89, 2996

Chen, S.-H, 1986. "Small Angle Neutron Scattering Studies of the Structure and Interaction in Micellar and Microemulsion Systems." Annual Review of Physical Chemistry, 37, 351

Chevalier, Y., and C. Chachaty, 1985. "Hydrocarbon Chain Conformation in Micelles. A Nuclear Magnetic Relaxation Study." Journal of Physical Chemistry, 89, 875

Clarke, J. H. R., and D. Brown, 1986. "Molecular Dynamics Computer Simulation of Chain Molecule Liquids. I. The Coupling of Torsional Motions to Translational Diffusion." Molecular Physics, 58, 815

Degiorgio, V., 1983. "Nonionic Micelles." In Physics of Amphiphiles: Micelles Vesicles, and Microemulsions; V. Degiorgio and M. Corti, eds; North–Holland, Amsterdam

Dill, K. A., 1982. "Configurations of the Amphiphilic Molecules in Micelles." Journal of Physical Chemistry, 86, 1498

Dill, K. A., 1984a. "Molecular Organization in Amphiphilic Aggregates." In Surfactants in Solution, Vol. 1; K. L. Mittal and B. Lindmann, eds.; Plenum Press, New York

Dill, K. A., 1985. "Reply to F. M. Menger." Nature, 313, 603

Dill, K. A., and P. J. Flory, 1980. "Interphases of Chain Molecules: Monolayers and Lipid Bilayer Membranes." Proceedings of the National Academy of Sciences U.S.A., 77, 3115

Dill, K. A., and P. J. Flory, 1981. "Molecular Organization in Micelles and Vesicles." Proceedings of the National Academy of Sciences U.S.A, 78, 676

Dill, K. A., D. E. Koppel, R. S. Cantor, J. A. Dill, D. Bendedouch, and S. H.-Chen, 1984b. "The Molecular Conformations in Surfactant Micelles." Nature (London), 309, 42

Edberg, R., D. J. Evans, and G. P. Morriss, 1986. " Constrained Molecular Dynamics: Simulations of Liquid Alkanes with a New Algorithm." Journal of Chemical Physics, 84, 6933

Edberg, R., G. P. Morriss, and D. J. Evans, 1987. "Rheology of n–Alkanes by Nonequilibrium Molecular Dynamics." Journal of Chemical Physics, 86, 4555

Enciso, E., J. Alonso, N. G. Almarza, and F. J. Bermejo, 1989. "Statistical Mechanics of Small Chain Molecular Liquids. I. Conformational Properties of Modeled n–Butane." Journal of Chemical Physics, 90, 413

Evans, D. J., 1977. "On the Representation of Orientation Space." Molecular Physics, 34, 317

Farrell, R. A., 1988. "Thermodynamic Modeling and Molecular Dynamics Simulation of Surfactant Micelles." Ph. D. Dissertation, University of Florida

Frank, H. S., and M. W. Evans, 1945. "Free Volume and Entropy in Condensed Systems." Journal of Chemical Physics, 13, 507

Fromherz, P., 1981. "Micelle Structure: A Surfactant Block Model." Chemical. Phys. Lett, 77, 460

Gear, C. W., 1971. Computational Methods in Ordinary Differential Equations; Prentice–Hall, Englewood Cliffs, NJ.

Geiger, A., A. Rahman, and F. H. Stillinger, 1979. "Molecular Dynamics Study of the Hydration of Lennard–Jones Solutes." Journal of Physical Chemistry, 70, 263

Glew, D. N., 1962. "Aqueous Solubility and the Gas–Hydrates. The Methane–Water System." Journal of Physical Chemistry, 66, 605

Goldammer, E. V., and H. G. Hertz, 1970. "Molecular Motion and Structure of Aqueous Mixtures with Nonelectrolytes as Studied by Nuclear Magnetic Relaxation Methods." Journal of Physical Chemistry, 74, 3734

Gruen, D. W. R., 1981. "The Packing of Amphiphile Chains in a Small Spherical Micelle." Journal of Colloid and Interface Science, 84, 281

Gruen, D. W. R., 1985a. "A Model for the Chains in Amphiphilic Aggregates. 1. Comparison with a Molecular Dynamics Simulation of a Bilayer." Journal of Physical Chemistry, 89, 146

Gruen, D. W. R., 1985b. "A Model for the Chains in Amphiphilic Aggregates. 1. Thermodynamics and Experimental Comparisons for Aggregates of Different Shape and Size." Journal of Physical Chemistry, 89, 153

Haan, S. W., and L. R. Pratt, 1981a. "Monte Carlo Study of a Simple Model for Micelle Structure." Chemical Physics Letters, 79, 436

Haan, S. W., and L. R. Pratt, 1981b. "Errata of 79, 436." Chemical Physics Letters, 81, 386

Haile, J. M., 1980. A Primer on the Computer Simulation of Atomic Fluids by Molecular Dynamics, Unpublished.

Haile, J. M., and J. P. O'Connell, 1984. "Internal Structure of a Model Micelle via Computer Simulation." Journal of Physical Chemistry, 88, 6363.

Hartley, G. S., 1935. Transactions of The Faraday Society, 31, 31 "The Application of the Debye–Huckel Theory to Colloidal Electrolytes"

Hayter, J. B., M. Hayoun, and T. Zemb, 1984. "Neutron Scattering Study of Pentanol Solubilization in Sodium Octanoate Micelles." Colloid and Polymer Science, 262, 798

Hayter, J. B., and J. Penfold, 1981. "Self–Consistent Structural and Dynamic Study of Concentrated Micelle Solutions." Journal of the Chemical Society, Faraday Transactions 1, 77, 1851

Hayter, J. B., and T. Zemb, 1982. "Concentration–Dependent Structure of Sodium Octanoate Micelles." Chemical Physics Letters, 93, 91

Helfland, E., 1979. "Flexible vs Rigid Constraints in Statistical Mechanics." Journal of chemical Physics, 71, 5000

Jönsson, B., O. Edholm, and O. Teleman, 1986. "Molecular Dynamics Simulation of a Sodium Octanoate Micelle in Aqueous Solution." Journal of Chemical Physics, 85, 2259

Jorgensen, W. L., 1981a. "Internal Rotation in Liquid 1,2–Dichloroethane and n–Butane." Journal of the American Chemical Society, 103, 677

Jorgensen, W. L., 1981b. "Pressure Dependence of the Structure and Properties of Liquid n–Butane." Journal of the American Chemical Society, 103, 4721

Jorgensen, W. L., 1981c. "Transferable Intermolecular Potential Functions for Water, Alcohols and Ethers. Application to Liquid Water." Journal of the American Chemical Society, 103, 335

Jorgensen, W. L., 1982. "Revised TIPS for Simulations of Liquid water and Aqueous Solutions." Journal of Chemical Physics, 77, 4156

Jorgensen, W. L., R. C. Binning, and B. Bigot, 1981e. "Structure and Properties of Organic Liquids: n–Butane and 1,2–Dichloroethane and Their Conformational Equilibria." Journal of the American Chemical Society, 103, 4393

Jorgensen, W. L., J Chandrasekhar, J. Madura, W. Impey, and M. Klein, 1983. "Comparison of Simple Potential Functions for Simulating Liquid Water." Journal of Chemical Physics, 79, 926

Jorgensen, W. L., J. D. Madura, and C. J. Swenson, 1984. "Optimized Intermolecular Functions for Liquid Hydrocarbons." Journal of the American Chemical Society, 106, 6638

Jorgensen, W. L., J. Gao, and C. Ravimohan, 1985. "Monte Carlo Simulations of Alkanes in Water: Hydration Numbers and the Hydrophobic Effect." Journal of Physical Chemistry, 89, 3470

Jorgensen, W. L., and M. Ibrahim, 1981d. "Structure and Properties of Organic Liquids: n–Alkyls Ethers and Their Conformational Equilibria." Journal of the American Chemical Society, 103, 3976

Lindman, B., O. Söderman, and H. Wennerström, 1987. "NMR Studies of Surfactant Systems" In Surfactant Solutions, New Methods of Investigation; Raoul Zana ed.; Dekker, New York

Matsouka, O., E. Clementi, and Y. Yoshimine, 1976. "CI Study of the Water Dimer Potential Surface." Journal of Chemical Physics, 64, 1351

Mehrotra, P. K., and D. L. Beveridge, 1980. "Structural Analysis of Molecular Solutions Based on Quasi–Component Distribution Functions." Journal of The American Chemical Society, 102, 4287

Menger, F. M., 1979. "On The Structure of Micelles." Accounts of Chemical Research, 12, 111

Menger, F. M., 1985. "Molecular Conformations in Surfactant Micelles." Nature, 313, 603

Muller, A., B. Krebs, A. Fadini, O. Glemser, S. J. Cyvin, J. Brunvoll, B. N. Cyvin, I. Elvebredd, G. Hagen, and B. Vizi, 1968. "Mean Amplitudes of Vibration, Force Constants and Coriolis Coupling Constants of $ZXY_2(C_{2v})$ and $ZXY_3(C_{3v})$ Type Molecules and Ions." Zeitschrift fur Naturforschung A, 23a, 1656

Nemethy, G., and H. A. Scheraga, 1962. "Structure of Water and Hydrophobic Bonding in Proteins." Journal of Chemical Physics, 36, 3401

Okazaki, S., K. Nakanishi, H. Touhara, N. Watanabe, and Y. Adachi, 1981. "A Monte Carlo Study on the Size Dependence in Hydrophobic Hydration." Journal of Chemical Physics, 74 5863

Owenson, B., and L. R. Pratt, 1984. "Molecular Statistical Thermodynamics of Model Micellar Aggregates." Journal of Physical Chemistry, 88, 2905

Pitzer, K.S., 1940. "The Vibration Frequencies and Thermodynamic Functions of Long Chain Hydrocarbons." Journal of Chemical Physics, 8, 711

Rallison, J. M., 1979. "The Role of Rigidity Constraints in the Rheology of Dilute Polymer Solutions." Journal of Fluid Mechanics, 93, 251

Rao, M., and B. J. Berne, 1981. "Molecular Dynamic Simulation of the Structure of Water in the Vicinity of a Solvated Ion." Journal of Physical Chemistry, 85, 1498

Rapaport, D. C., and H. A. Scheraga, 1982. "Hydration of Inert Solutes. A Molecular Dynamics Study." Journal of Physical Chemistry, 86, 873

Rebertus, D. W., B. J. Berne, and D. Chandler, 1979. "A Molecular Dynamics and Monte Carlo Study of Solvent Effects on The Conformational Equilibrium of n–Butane in CCl_4." Journal of Chemical Physics, 70, 3395

Remerie, K., W. F. Van Gunsteren, J. P. M. Postma, H. J. C. Berendsen and J. B. F. N. Engberts, 1984. "Molecular Dynamics Computer Simulation of the Hydration of Two Simple Organic Solutes. Comparison with the Simulation of an Empty Cavity." Molecular Physics, 53, 1517

Ryckaert, J. P., and A. Bellemans, 1975. "Molecular Dynamics of Liquid n–Butane Near its Boiling Point." Chem. Phys. Lett., 30, 123

Ryckaert, J. P., and A. Bellemans, 1978. "Molecular Dynamics of Liquid Alkanes." Discuss. Faraday Soc., 66, 95

Stillinger, F. H., and A. Rahman, 1974. "Improved Simulation of Liquid Water by Molecular Dynamics." Journal of Chemical Physics, 60, 1545

Stillinger, F. H., and A. Rahman, 1978. "Revised Central Force Potentials for Water." Journal of Chemical Physics, 68, 666

Strauch, H. J., and P. T. Cummings, 1989. "Computer Simulation of the Dielectric Properties of Liquid Water." Molecular Simulation, 2, 89

Szczepanski, R., and G. C. Maitland, 1983. "Influence of Flexibility on the Properties of Chain Molecules." In Molecular–Based Study of Fluids, Advances in Chemistry Series, 204; J. M. Haile, and G. A. Mansoori eds.; Washington

Tabony, J., 1984. "Structure of the Polar Head Layer, and water Penetration in a Cationic Micelle. Contrast Variation Neutron Small Angle Scattering Experiments." Molecular Physics, 51, 975

Tanaka, H., 1987. "Integral Equation and Monte Carlo Study on Hydrophobic Effects: Size Dependence of Apolar Solutes on Solute–Solute Interactions and Structures of Water." Journal of Chemical Physics, 86, 1512

Taupin, C., and M. Dvolaitzky, 1987. "Spin Labels." In Surfactant Solutions, New Methods of Investigation; Raoul Zana ed.; Dekker, New York

Toxvaerd, S., 1987. "Comment on Constrained Molecular Dynamics of Macromolecules." Journal Of Chemical Physics, 87, 6140

Toxvaerd, S., 1988. "Molecular Dynamics of Liquid Butane." Journal of Chemical Physics, 89, 3808

Van Gunsteren, W. F., J. C. Berendsen, and J. A. C. Rullmann, 1981. "Stochastic Dynamics for Molecules with Constraints Brownian Dynamics of n–Alkanes." Molecular Physics, 44, 69

Vilallonga, F. A., R. J. Koftan, and J. P. O'Connell, 1982. "Interfacial Tensions and Partition Coefficients in Water and n–Heptane Systems Containing n–Alkanols, Alkylketones, Alkylamides, and Alkylmonocarboxylic Acids." Journal of Colloid and Interface Science, 90, 539

Ulmius, J., and B. Lindmann, 1981. "^{19}F NMR Relaxation and Water Penetration in Surfactant Micelles." Journal of Physical Chemistry, 85, 4131

Watanabe, K., and H. C. Andersen, 1986. "Molecular Dynamics Study of the Hydrophobic Interaction in an Aqueous Solution of Krypton." Journal of Physical Chemistry, 90, 795

Watanabe, K., M. Ferrario, and M. L. Klein, 1988. "Molecular Dynamics Study of a Sodium Octanoate Micelle in Aqueous Solution." Journal of Physical Chemistry, 92, 819

Weber, T. A., 1978. "Simulation of n–Butane Using a Skeletal Alkane Model." Journal of Chemical Physics, 69, 2347

Weiner, S. J., P. A. Kollman, D. A. Case, U. C. Singh, C. Ghio, G. Alagona, S. Profeta, and P. Weiner, 1984. "A New Force Field for Molecular Mechanical Simulation of Nucleic Acids and Proteins." Journal of The American Chemical Society, 106, 765

Wielopolski, P. A., and E. R. Smith, 1986. "Dihedral Angle Distribution in Liquid n–Butane: Molecular Dynamics Simulations." Journal of Chemical Physics, 84, 6940

Woods, M. C., J. M. Haile, and J. P. O'Connell, 1986. "Internal Structure of a Model Micelle via Computer Simulation. 2. Spherically Confined Aggregates with Mobile Head Groups." Journal of Physical Chemistry 90, 1875

Zana, R., 1987. "Luminescence Probing Methods." In Surfactant Solutions, New Methods of Investigation; Raoul Zana ed.; Dekker, New York

Zemb, T., and C. Chachaty, 1982. "Alkyl Chain Conformations in a Micellar System From the Nuclear Spin Relaxation Enhanced by Paramagnetic Ions." Chemical Physics Letters, 88, 68

Zemb, T., and P. Charpin, 1985. "Micellar Structure From Comparison of X–ray and Neutron Small–Angle Scattering." Journal de Physique, 46, 249
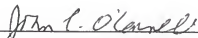
Zichi, D. A., and P. J. Rossky, 1986a. "Molecular Conformational Equilibria in Liquids." Journal of Chemical Physics, 84, 1712

Zichi, D. A., and P. J. Rossky, 1986b. "Solvent Molecular Dynamics in Regions of Hydrophobic Hydration." Journal of Chemical Physics, 84, 2814
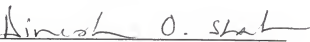
BIOGRAPHICAL SKETCH

Sami Karaborni was born in 1964 in Sousse, Tunisia, the son of Tijani Karaborni and the former Jamila Kedadi. He graduated from the Lyçee de Garçons de Sousse in 1982. After pursuing a brief intensive English program in State College, Pennsylvania, he joined the Pennsylvania State University College of Engineering in December of 1982. In 1986 he received with high distinction the degree of Bachelor of Science in chemical engineering. Subsequently, he joined the Graduate Program at the University of Florida, receiving a Master of Science degree in 1987.
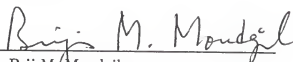
I certify that I have read this study and that in my opinion it conforms to acceptable standards of scholarly presentation and is fully adequate, in scope and quality, as a dissertation for the degree of Doctor of Philosophy.

John P. O'Connell, Chairman
Professor of Chemical Engineering

I certify that I have read this study and that in my opinion it conforms to acceptable standards of scholarly presentation and is fully adequate, in scope and quality, as a dissertation for the degree of Doctor of Philosophy.

Dinesh O. Shah, Co–Chairman
Professor of Chemical Engineering

I certify that I have read this study and that in my opinion it conforms to acceptable standards of scholarly presentation and is fully adequate, in scope and quality, as a dissertation for the degree of Doctor of Philosophy.

Brij M. Moudgil
Professor of Materials Science
and Engineering

I certify that I have read this study and that in my opinion it conforms to acceptable standards of scholarly presentation and is fully adequate, in scope and quality, as a dissertation for the degree of Doctor of Philosophy.
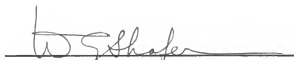
Gerald B. Westermann–Clark
Associate Professor of Chemical
Engineering

This dissertation was submitted to the Graduate Faculty of the College of Engineering and to the Graduate School and was accepted as partial fulfillment of the requirements for the degree of Doctor of Philosophy.

May, 1990

Winfred M. Phillips
Dean, College of Engineering

Madelyn M. Lockhart
Dean, Graduate School